FINAL TECHNICAL PROGRESS REPORT

Title: Nanostructured High Performance Ultraviolet and Blue Light Emitting Diodes for Solid State Lighting*
Type of report: Final
Reporting Period: October 1, 2003 to March 31, 2007
Principal Authors: Professor Arto V. Nurmikko (Brown University) and Professor Jung Han (Yale University)
Date Report was Issued: June 29, 2007
DOE Award Number: DE-FC26-03NT41941

ABSTRACT

We report on research results in this project which synergize advanced material science approaches with fundamental optical physics concepts pertaining to light-matter interaction, with the goal of solving seminal problems for the development of very high performance light emitting diodes (LEDs) in the blue and near ultraviolet for Solid State Lighting applications. Accomplishments in the duration of the contract period include (i) new means of synthesizing AlGaN and InN quantum dots by droplet heteroepitaxy, (ii) synthesis of AlGaInN nanowires as building blocks for GaN-based microcavity devices, (iii) progress towards direct epitaxial alignment of the dense arrays of nanowires, (iv) observation and measurements of stimulated emission in dense InGaN nanopost arrays, (v) design and fabrication of InGaN photonic crystal emitters, and (vi) observation and measurements of enhanced fluorescence from coupled quantum dot and plasmonic nanostructures. The body of results is presented in this report shows how a solid foundation has been laid, with several noticeable accomplishments, for innovative research, consistent with the stated milestones.

TABLE OF CONTENTS

FINAL TECHNICAL PROGRESS REPORT 1
ABSTRACT 1
TABLE OF CONTENTS 2
EXECUTIVE SUMMARY 4
I INTRODUCTION 5
II EXPERIMENAL 5
III RESULTS AND DISCUSSION 6
III.A Synthesis of 410 nm light emitting medium 6
III.B GaN Quantum Dots 8
III.C InN quantum dots 9
III.D Synthesis of AlGaInN Nanowires 13
III.E AlN/GaN DBR mirror with R>95% 20
III.F Nano ELO and Selective Area Epitaxy 20
III.G Photonic Crystal 21
III.H Nanostructured light emitting medium 23
III.I Hybrid Organic-Inorganic light emitting medium for green LEDs 26
IV MILESTONE SUMMARY 333
V LIST OF PUBLICATIONS AND PRESENTATIONS 344
REFERENCES 2036

LIST OF GRAPHICAL MATERIALS

All graphical materials are imbedded within the main body of this report.

EXECUTIVE SUMMARY

The aim of this research project at Brown and Yale Universities is to synergize advanced material science approaches with fundamental optical physics concepts pertaining to light-matter interaction, with the goal of solving fundamental efficiency problems so as to enable the development of very high performance light emitting diodes (LEDs) in the blue and near ultraviolet for Solid State Lighting applications, covering the spectral regime of approximately 370-480 nm. Our work is directed towards novel, highly adaptable device concepts that enable their flexible utilization and matching to the broad spectrum of approaches and requirements that pertain to contemporary solid state lighting approaches. The material base of the light emitters if formed from nanostructured gallium nitride and related semiconductor heterostructures, which are enclosed by mesoscopic optical confinement and light emitting enclosures for efficient extraction of optical energy. The ultimate goal of the research is to reach the goal of a highly wall-plug efficient, high optical power device by concentrating on two specific, closely coupled performance dictating elements within the LED.

The research program has been organized in the following way: First, in ongoing work we are synthesizing nanostructured active media to enhance the internal radiative efficiency utilizing special concepts in epitaxial growth for growing quantum dots and quantum wires. Second, the research has also focused focus on the design and fabrication of advanced photonic confinement structures, which encase the nanostructured active medium for enhancing the spontaneous emission by strengthening light-matter interaction at a fundamental level and for efficiently extracting and distributing the photons for delivery into specific geometrical radiation patterns by design.

Below we summarize the progress made during the second year of the project. The body of results is presented clearly indicates that a solid foundation has been laid, in additional to several noticeable accomplishments, for reaching the stated milestones in the coming years. Specifically we have made substantially advances in the synthesis of zero- and one-dimensional GaN nanostructures, established the building blocks for making GaN-based microcavity devices, and demonstrated a top-down approach to nano-scale photonic devices for enhanced spontaneous emission and light extraction.

I INTRODUCTION

A revolution in lighting regarding energy saving, component lifetime, and fixture versatility is anticipated if the traditional tube-based (incandescent and fluorescent) lamps can be replace by solid state LEDs. For this vision to become reality, a substantial gap in terms of light output between a standard incandescent bulb (1000~2000 lumens) and a single III-N LED chip (1~5 lumens) needs to be bridged. Engineering issues such as metal contacts, current spreading, and light extraction have to be addressed in scaling up the device area for increased optical output from a single chip. Of paramount importance is the identification and realization of an active medium capable of more efficient conversion of electron-hole pairs into photons, especially under higher-level current injection ($J=10^3 \sim 10^4$ A/cm^2). Carrier localization due to In-related compositional fluctuations in InGaN is attributed to the constraint of in-plane carrier diffusion, thus preserving and preventing the injected carriers from recombining at nonradiative dislocation sites. Such a benefit of localization diminishes at high-level injection as more carriers acquire a nature of extended electronic states and are consumed by nonradiative processes. A recent observation of a substantial decay in quantum efficiency at a modest injection level from state-of-the-art high power AlGaInN LEDs[1] served as a reminder of the necessity of innovative and creative material research for an efficient light-emitting medium.

In this report we summarize the progress and accomplishment made during the DOE Contract entitled "Nanostructured High Performance Ultraviolet and Blue Light Emitting Diodes for Solid State Lighting". Details of the experimental facilities and methodology are described in experimental section (II). The body of results is presented in Section III which clearly indicated that a solid foundation has been laid, in additional to several noticeable accomplishments, for reaching the stated milestones in the coming years. Specifically we have made substantially advances in the synthesis of zero- and one-dimensional GaN nanostructures, established the building blocks for making GaN-based microcavilty devices, and demonstrated a top-down approach to nano-scale phontic devices for enhanced spontaneous emission and light extraction.

II EXPERIMENAL

MOCVD growth was carried out in a horizontal reactor (Aixtron 200/4 HT-S) using trimethylgallium (TMGa), trimethylaluminum (TMAl), and ammonia (NH_3) as sources with hydrogen and nitrogen as carrier gases. Atomic force microscopy (AFM) was conducted using a Digital Instrument Nanoprobe III model with tapping mode. PL signal was collected using a 30 ns pulsed frequency-quadrupled solid laser emitting at 263 nm. Scanning electron microscopy (SEM) was performed using a LEO 1530 Field Emission SEM. Chemical composition is determined by energy dispersive x-ray spectroscopy (EDS) that is embedded in the SEM. High-resolution transmission electron microscopy (TEM) and electron diffraction (ED) were performed using a FEI Tecnai 20 Field Emission TEM. Scanning energy dispersive x-ray spectrometry (EDS) was carried out in a Philips CM-12 TEM with a nominal beam diameter of 50 nm.

III RESULTS AND DISCUSSION

III.A Synthesis of 410 nm light emitting medium

After a series of InGaN multiple quantum well calibration growths in December of 2003, we initiated the effort of 410 nm VCSEL in January of 2004 toward the demonstration of electrically injected surface emitting devices. Under optical pumping, a sample with ten InGaN/GaN MQWs exhibited amplified spontaneous emission (ASE, Fig. 1) under relatively low pumping power, indicating the quality of the active region (InGaN MQWs) is sufficient to produce optical gains. Atomistic morphology was study and optimized by varying the growth pressure during the MOCVD process (from 200 to 300 mbar). P-doping of GaN was established and high-brightness LED at 410 nm is achieved (Fig. 1).

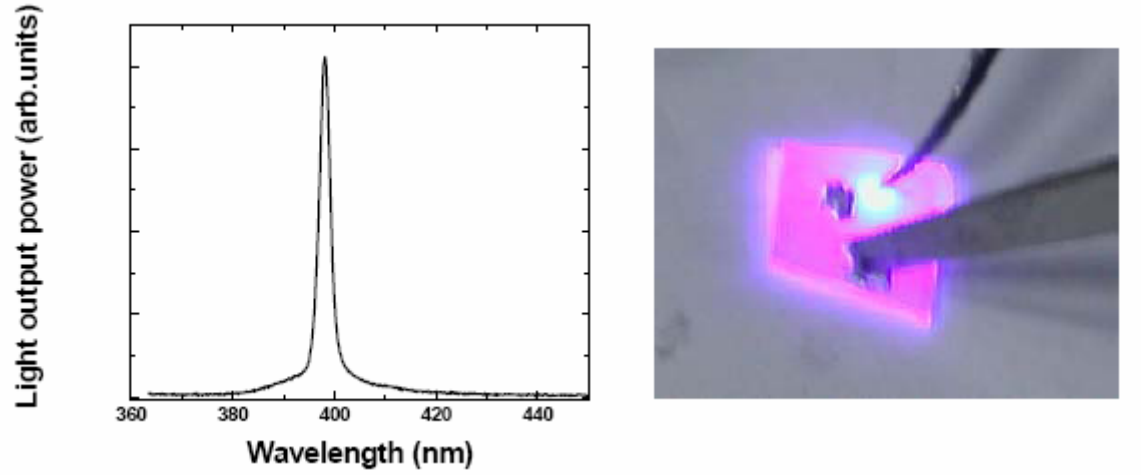

Fig 1. (left) Amplified spontaneous emission from an optically-pumped InGaN MQW structure, and (right) photograph of a 410nm InGaN LED.

Two factors which influence the optical properties of InGaN MQW are band-filling (Moss-Burstein effect) and built-in electric field (piezoelectric polarization effect). One way to study and differentiate these two effects is to vary the excitation power. Two samples were grown at the identical condition except with different growth time, therefore different well thickness. The QW growth time of 0316A is 50% longer than that of 0315C. As the excitation power increases, the PL peak position was blue-shifted in both samples (Fig 2a), however, the value of peak shift in 0316A (100 meV) was twice larger than that of 0315C (50 meV). Fig 1b shows the variation of FWHM of PL peak as a function of excitation power; the V-shaped dependence was appeared in 0316A (wider QW than 3 nm), however, there's only linear dependence in 0315C. By increasing excitation power, only band filling effect would affect on optical properties in case of thin QW, however, built-in electric field as well as band filling affect on optical properties in wider QW so that the FWHM shows V-shaped dependence as in the case of 0316A. Such kind of plots give us a precise determination of the dimension of the InGaN MQWs

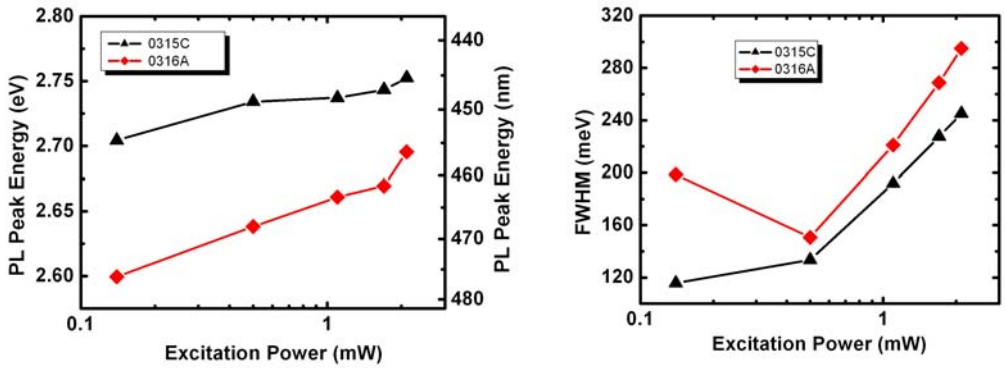

Fig 1. (a) Peak energy vs excitation power for two InGaN MQW samples of different well width, and (b). FWHM of PL vs excitation power for two InGaN MQW samples of different well width.

Temperature-dependent PL study of InGaN MQW: We have also studied the temperature dependence of PL from InGaN MQWs from 4 to 300k. Fig 3a shows the PL spectrum at different temperatures for a "violet" and a "blue-green" MQW. The corresponding shift in peak energy versus temperature is plotted in Fig 2b. S-shape" temperature dependence was shown in all InGaN/GaN MQW samples due to either thermalization of excitons, however, the degree of localization fitted from Varshini's equation was quite small (less than 10 meV).

From the plot of integrated intensity vs. 1/T (Fig 4), the only nonradiative pathway exists in all MQW samples and the value of activation energy was around 13~15 meV. From the literature, general reported value of activation energy was around 35~40 meV. The apparently low activation energy in our InGaN QWs might be due to the employment of low growth temperatures and slow growth rate (low gas delivery efficiency) which contribute to the presence of point defects.

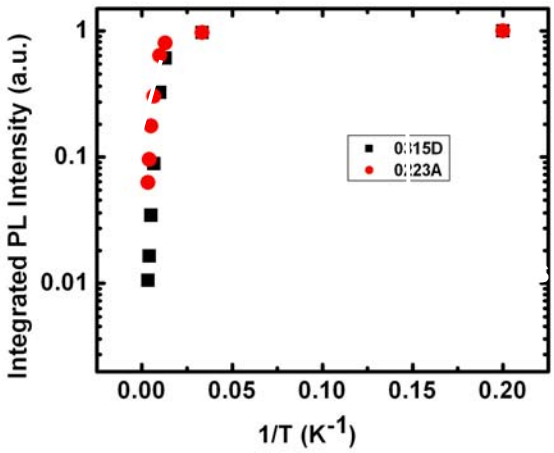

Fig 3 Arrenhius plot of PL intensity showing the activation behavior.

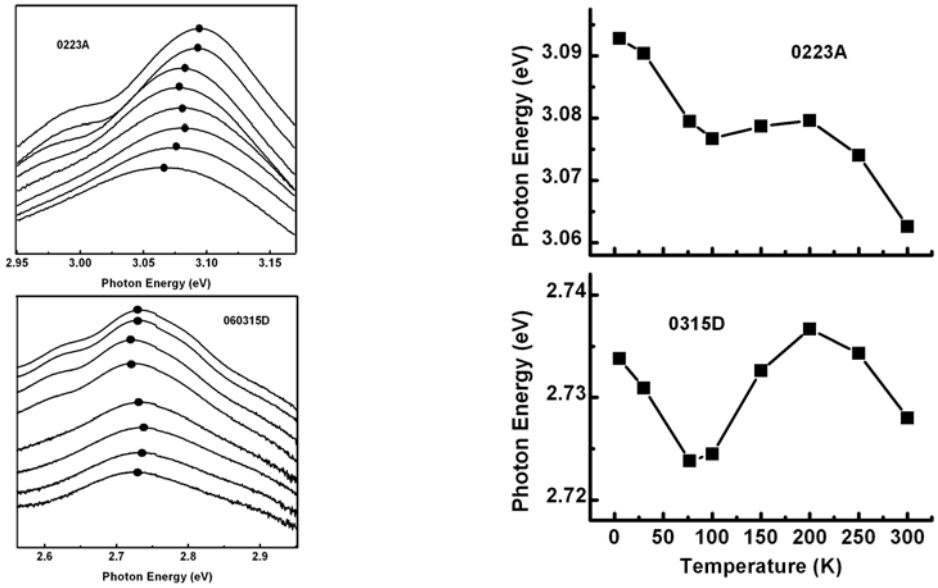

Fig 4. (a) Temperature-dependent PL spectrum for two InGaN MQW samples, and (b) peak energy vs temperature for two InGaN samples.

III.B GaN Quantum Dots

Near and above its melting point, metallic thin film transforms into nanoscale liquid droplets, a phenomenon that does not require the presence of strain mismatch or surfactant. The formation of metal droplets due to surface tension presents an alternative route to semiconductor nanostructures by converting the droplets into crystalline QDs. Koguchi et al.[2] has demonstrated the formation of nanometer Ga droplets on GaAs substrates and the conversion into GaAs QDs through an exposure to arsenic vapor. Kawasaki et al.[3] and Hu et al.[4] have reported the preparation of GaN QDs on, respectively, AlGaN and SiC by droplet conversion using gas source MBE. Only low temperature luminescence was observed in these samples; a deviation of microscopic stoichiometry was identified as a factor compromising the recombination efficiency. Last year we demonstrated that gallium droplet heteroepitaxy (DHE) is a valid path toward the flexible synthesis of GaN QDs with high optical efficacy. The formation of Ga droplets, including the nucleation dynamics and kinetics, had been examined at the atomic scale. The conversion of gallium droplets upon exposure to ammonia proceeds with two competing mechanisms, a liquid-phase-epitaxy-like crystallization of quantum dots and the diffusion-based two-dimensional growth of GaN layers, both can be regulated by surface kinetics. Photoluminescence (PL) at 345 nm at room temperature suggests that the converted QDs are optically active and can be a candidate for ultraviolet emitters.

This year we extended our DHE study to the alloy system of AlGaInN. In the formation of AlGaN quantum dots, we first mixed in the gas phase the Ga and Al

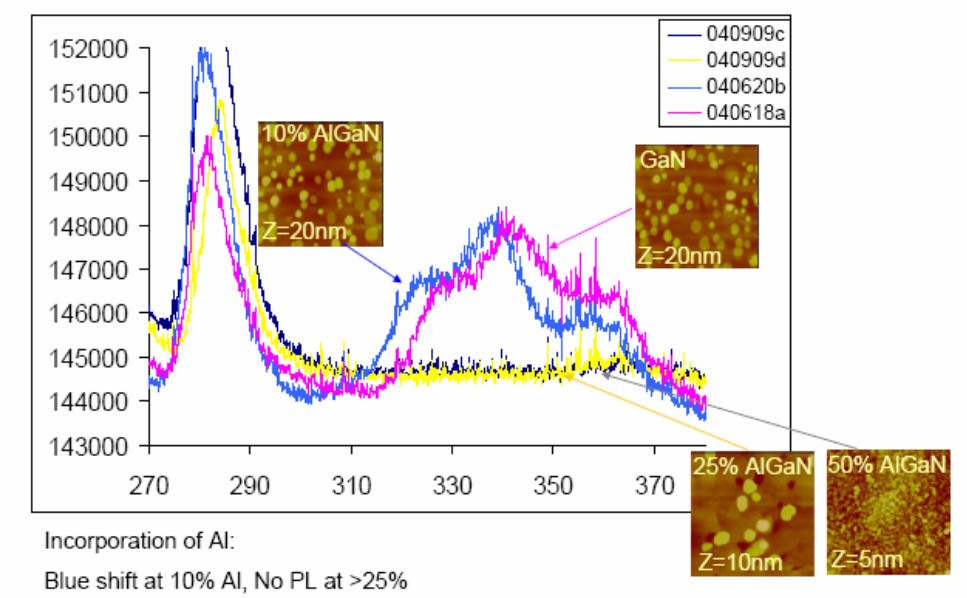

Fig 5. Room temperature PL from GaN and AlGaN quantum dots with varying Al compositions.

precurors and create metallic droplets on AlGaN surface.

Conversion of Al/Ga nanodroplets into AlGaN quantum dots was preformed by exposing the Al/Ga droplets to ammonia flow immediately after the interruption of TMAl and TMGa flow, followed by a rapid cooling of the samples under NH_3 flow. The conversion process represents interplay between several competing mechanisms. The first is the reaction of nitrogen with Al/Ga nanodroplets, resulting in the formation of a supersaturated solution and consequently the crystallization of AlN/GaN at the droplet/AlGaN interface. On the other hand, the transition from nanodroplets to crystal can proceed differently when Ga and Al adatoms have a high surface diffusion rate; the diminishing role of the surface tension as Al and Ga droplets solidify in the absence of a high compressive strain makes it possible for the Al and Ga atoms to diffuse out from the droplets and participate in a layer-by-layer growth.[5] It was discovered that, as the Al composition in the droplets increases above 40%, the conversion process proceeds with the formation of dispersive small grains intermixed with layered nucleation.

Optical properties of GaN obtained by DHE were investigated by PL with a 266 nm excitation source. Room-temperature PL spectra of AlGaN-capped QD samples are shown in Figure 5. To remove the ambiguity in PL peak designation, an $Al_{0.40}Ga_{0.60}N$ template is used which gives rise to a distinct peak at 280 nm. A blue shift in PL emission as we add 10% Al into GaN is consistent with the increase of the alloy bandgap. Above 20% of Al/Ga alloy, we were not able to observe any distinct PL.

III.C InN quantum dots

InN is a highly attractive group-III nitride semiconductor for future applications in high mobility transistor and near-infrared optoelectronics and as a constituent of Ga-rich InGaN alloys, which are now widely used in commercial optoelectronics in ultraviolet to green spectral range. However, InN and In-rich InGaN alloys are still at the stage of establishing growth techniques and basic physical properties such as bandgap and

effective mass.[6] Regarding bandgap of InN, the widely varying values in the range of 0.6-2.0 eV have been reported[7,8,9] and the origin of these variation is under much debate. O_N has been proposed as a candidate for the major residual donor species in InN,[10] and the incorporation of oxygen and the Burstein-Moss effect due to residual large carrier concentrations have been suggested as a possible origin of large discrepancy in the reported bandgap of InN.[11,12] It is expected that oxidation would easily occur for indium residue on surface in preference to nitridation by considering the large difference in the heat of formation of InN (34 kcal/mol)[13] compared with In_2O_3 (221 kcal/mol)[14] and Xu *et al*. reported the precipitation of In_2O_3 with less than 0.07 vol % in epitaxial InN films grown by molecular beam epitaxy (MBE).[15]

Since the lattice mismatch between InN and GaN (or AlN) is larger than 10%, the density of misfit dislocations at the hetero-interface between as-grown InN and GaN (or AlN) is very high[16] and these defects would deteriorate the quality of InN-based devices. One of the possible solutions to avoid this problem is to introduce InN-based nanostructures such as ultra-thin quantum wells,[16] quantum dots,[17] and nanowires[18] in active region. However, depending on the growth condition, there's still a possibility of oxide precipitation in InN nanostructures during growth and/or post-growth procedures because of high volatility of N_2 from InN surface[6,16] and high tendency for indium residue on surface to strongly chemisorb residual molecular oxygen.[14] In this letter, we report on the observation of oxide precipitates (bcc-In_2O_3) in InN nanostructures during metal-organic chemical vapor deposition (MOCVD) growth and/or post-growth procedures in H_2 ambient. InN was extremely unstable in H_2 ambient and the oxide precipitates were very similar to that expected from genuine InN nanostructures, which suggest a possibility of false detection.

Two sets of InN nanostructures were grown in commercial horizontal MOCVD reactors. Trimethylgallium (TMGa), trimethylindium (TMIn), and ammonia (NH_3) were used as Ga, In, and N sources. First set of InN nanostructures is a few monolayer (ML)-thick InN epitaxial layers grown on 2-μm-thick GaN/sapphire(0001) templates [growth temperature: 1080 ^oC] and the growth of InN was performed at 730 ^oC for 90 s. All growth conditions were fixed and TMIn (10 μmol/min) and NH_3 (4.0 slm) were supplied as precursors and N_2 carrier gas was used. Immediately after the InN growth, the TMIn was shut off and both NH_3 and N_2 carrier gas was still introduced during cooling procedure to 400 ^oC. Then, we varied cooling environment and examined the surface morphology and structural properties of InN layers with atomic force microscopy (AFM) and transmission electron microscopy (TEM). Second set of InN nanostructures was grown on top of 20-nm-thick cubic GaN (c-GaN)/GaP(100) templates [growth temperature: 520 ^oC] to examine the thermal stability of InN in H_2 ambient. The growth temperature of InN was varied in the range of 450~550 ^oC and H_2 carrier gas was introduced throughout the InN growth with NH_3. Immediately after the InN growth, H_2 carrier gas was replaced to N_2 and both NH_3 and N_2 carrier gas were introduced during cooling process to room temperature (RT). The growth rate of InN was controlled by TMIn flow rate and NH_3 flow rate was fixed at 3.75 slm. The TMIn flow rates were 7.5 and 15 μmol/min, and the corresponding growth times were 45 and 22.5 min, respectively, to keep the total amount of deposition from the gas-phase sources a constant (i.e. TMIn flow rate x deposition time = constant) in all InN growth at a certain growth

temperature. The effects of change in growth conditions on the surface morphology were investigated by AFM and scanning electron microscopy (SEM) and the structural properties were examined by TEM.

At first, we grew a few ML-thick InN on GaN template to see the surface morphology of the bare InN layer. The surface morphology of 2-μm-thick GaN layer used as a substrate for InN growth was observed by AFM and typical step-flow like feature of atomically flat GaN surface was appeared (not shown here). After 90 s InN deposition, the sample was cooled down to RT with flowing both NH_3 and N_2 carrier gas and the sample surface shows the stepped 2 dimensional (2D) morphology with the formation of 2D disk-shaped structure on terraces, as shown in Fig. 6(a). Heights of 2D disk-shaped structures were about 3~5 Å measured by AFM, equivalent to 1~2 ML of InN unit cell and their diameters were less than 200 nm.[19] However, in case of the sample with different cooling environment, the surface morphology of InN was greatly changed, as shown in Fig. 6(b). Surprisingly, QD-like structures with a density of 2.5 x 10^9 cm^{-2} appeared on InN surface and most of them existed on 2D disk-shaped structure. Only difference in growth procedure in this sample is that the NH_3 was shut off and input carrier gas changed to H_2 immediately after the substrate temperature reaches to 400 ^oC during cooling process.

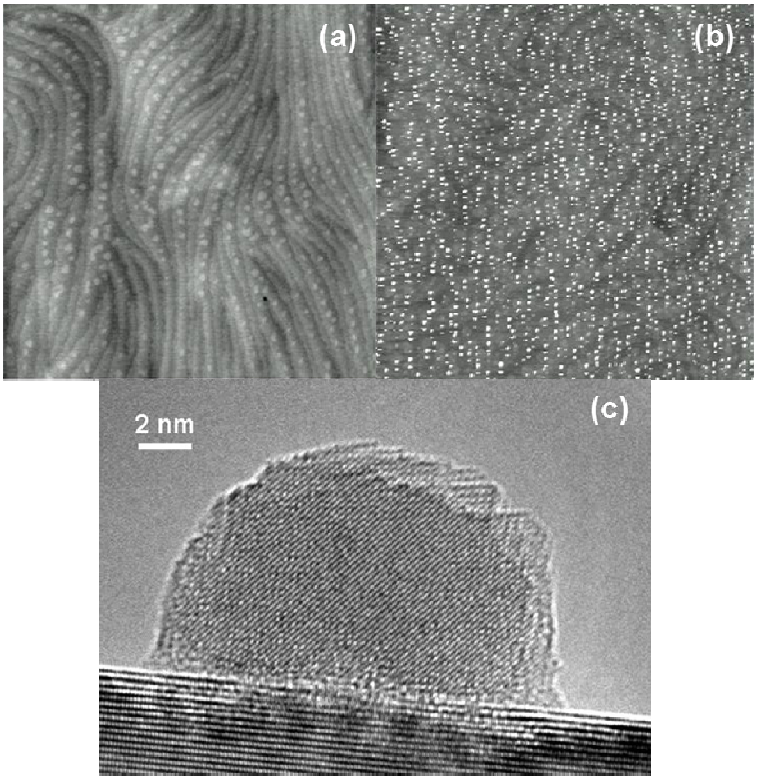

Fig. 6. 4 μm x 4 μm AFM images of a few ML-thick InN layers on GaN templates with a cooling environment of (a) NH_3 and N_2 carrier gas to RT, (b) NH_3 and N_2 carrier gas to 400 ^oC, followed by switch to only H_2 carrier gas to RT and (c) cross-section TEM image of In_2O_3 formed on InN layer.

From the cross-section high resolution (HR) TEM image as shown in Fig. 6(c), we found that the QD-like structures on InN surface have a different texture with underlying

GaN template and it turns out to be bcc-In_2O_3 instead of InN. The inter-planar spacing of HR lattice fringe image of In_2O_3 was ~2.9 Å and this corresponds to the reported lattice constant of bcc-In_2O_3 (222),[20] which is in good agreement with a preferential orientation of In_2O_3 formed by thermal oxidation of InN.[21] We suppose that decomposition and desorption of N_2 from InN surface greatly enhanced in H_2 ambient during cooling process and indium residue on the surface would strongly chemisorb residual molecular oxygen,[14] resulting in In_2O_3 formation mainly on 2D disk-shaped structures.

To examine thermal stability of InN in H_2 ambient, we grew phase pure cubic InN (c-InN) dots with H_2 carrier gas on 20-nm-thick c-GaN/GaP (100) templates at constant amount of deposition from the gas-phase sources but different temperature and growth rate. Growth proceeded through sparse dots' nucleation and coalescence and the increase of growth temperature from 450 ^oC to 550 ^oC decreased the dot density and increased the dot size at both growth rates, indicating thermally activated growth mode of InN. The calculation of growth rate of c-InN dots was based on the assumption of the shape of c-InN dots as a perfect hemisphere. The results are shown in Fig. 7. Higher growth temperature leads to lower growth rate, indicating the strong thermal decomposition of InN during growth and the activation energy is measured to be ~ 0.28 eV on the Arrhenius plot. This value is one order of magnitude smaller than reported N_2 desorption activation energy of InN (or GaN) in a vacuum.,[22,23] The introduction of H_2 carrier gas during InN growth leads to extremely low thermal stability of InN and this can be explained by thermodynamic calculations on the role of hydrogen in terms of layer etching and reduction of nitrogen sticking coefficient.[24]

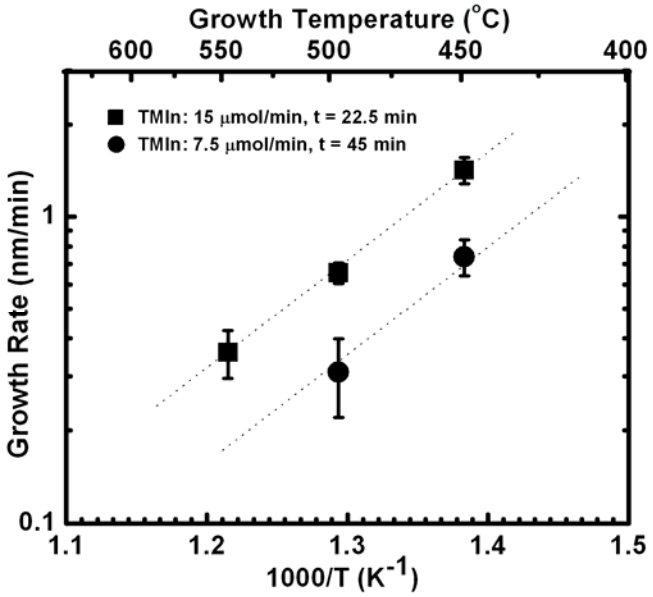

Fig. 7. Arrhenius plot of N_2 desorption-controlled growth rate of c-InN dots vs. substrate temperature at constant amount of deposition from the gas-phase sources.

Bcc-In_2O_3 precipitates were also observed in c-InN dots grown in H_2 ambient. They coexist in InN matrix with orientation relationship of $[011]_{In2O3}$ // $[011]_{InN}$ and $[100]_{In2O3}$ // $[100]_{InN}$ and there's no measurable detection of hexagonal InN at all. Figure 8(a)

shows a HRTEM image taken for c-InN dots grown at 450 °C with TMIn flow rate of 15 μmol/min. Figure 8(b) shows an electron diffraction pattern (EDP) obtained from the interface between c-GaN and GaP (100) substrate and we can't detect any measurable oxide precipitates in 20-nm-thick c-GaN layers. However, an EDP shown in Fig. 8(c) obtained only from c-InN dots shows the coexistence of bcc-In_2O_3 in c-InN matrix. The coincidence between the diffraction spot (400) in In_2O_3 and (200) in c-InN indicates that the spacing between {400} planes in bcc-In_2O_3 (~2.53 Å)[20] nearly equals to the spacing between {200} planes in c-InN (~2.49 Å).[25] In this work, while (Al)GaN could be grown without obvious oxidation using the MOCVD, but InN showed easily oxidizable nature, as Yoshimoto *et al*. pointed out in MBE growth.[11] It should be noted that there's a possibility of formation of oxide precipitates in InN during MOCVD growth even in an inert gas environment such as N_2 because H_2 carrier gas generally introduced to the reactor chamber for subsequent (Al)GaN growth and H_2 produced by the decomposition of NH_3 can play the same role.[24,26]

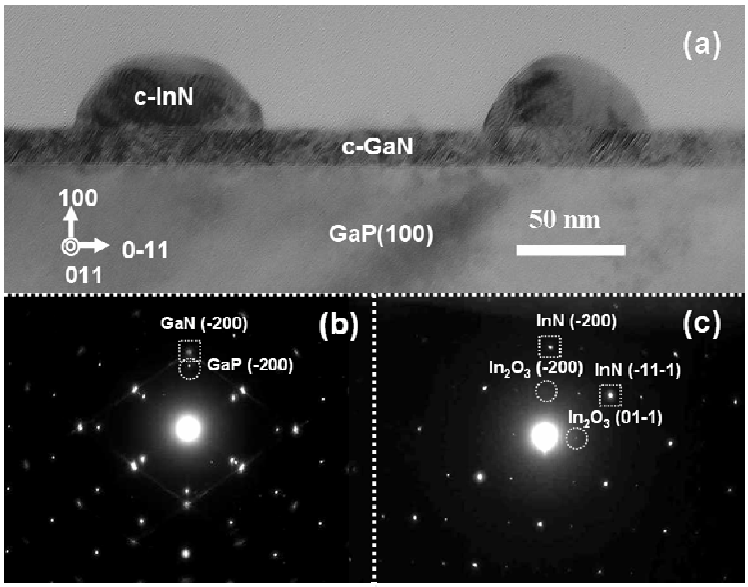

Fig. 8. (a) Cross-section TEM image of c-InN dots grown at 450 °C with TMIn flow rate of 15 μmol/min on 20-nm-thick c-GaN/GaP (100), (b) an electronic diffraction pattern (EDP) of the interface between c-GaN buffer and GaP (100) substrate, and (c) an EDP of the c-InN dots.

III.D Synthesis of AlGaInN Nanowires

To date the synthesis of GaN nanowires are performed primarily by a near-equilibrium, tube furnace technique which does not offer optimum control or flexibility. In this letter we report our observations in preparing III-N nanowires using a conventional MOCVD system. In addition to demonstrating GaN and AlN nanowires from a cold-wall, commercial platform, which has not been reported to our knowledge, we outline the critical issues of nanowire synthesis and present specific solutions. The versatility of using MOCVD for nanowire synthesis is illustrated by the fabrication of three-dimensional (3D) GaN/AlN nano-trees.

The basic principle of VLS mechanism for anisotropic growth of 1D nanostructures was summarized by Wagner.[4] Prerequisites that were identified include: (1) A sizable

disparity in reaction kinetics between regular vapor-solid (VS) and the VLS mechanisms, thus mandating a low supersaturation for growth selectivity; (2) the creation and retention of liquid droplets to facilitate adsorption and incorporation of vapor phase species; and (3) the need to have nucleation sites with appropriate crystallographic orientations conducive to the minimization of surface energies. Criterion (1) helps to elucidate the popularity and success in the synthesis of GaN nanowires through hot-wall, flow-tube furnace chamber in which elemental Ga source is placed upstream of catalyst-treated substrates.[27] The proximity of a desorptive source to an adjacent growth surface spontaneously creates an ambient that is close to thermodynamic equilibrium. Favorable conditions for nanowires growth (under low supersaturation) is empirically derived by adjusting the relative positioning between the Ga boat and substrate due to spatial gradients in temperature and Ga flux. On the other hand, modern MOCVD involves a much different and complex process in which organometallic precursors (undersaturated even at room temperature) are transported in vapor phase with minimum dissociation to the vicinity of growth surface. The precursors then undergo rapid pyrolysis decomposition upon entering the heated zone near surface (thermal boundary layer), creating a highly inhomogeneous profile and a mass-transport limited growth process.[28]

During the first year of the current DOE project, we have demonstrated the synthesis of GaN nanowires by MOCVD and provided very detailed structural analysis (Fig. 9). In the 2nd year of this DOE project we carried out the synthesis of alloy nanowires and explored the possibility of aligning the nanowires through crystallographic epitaxy in order to incorporate these nanowires into conventional light emitting devices.

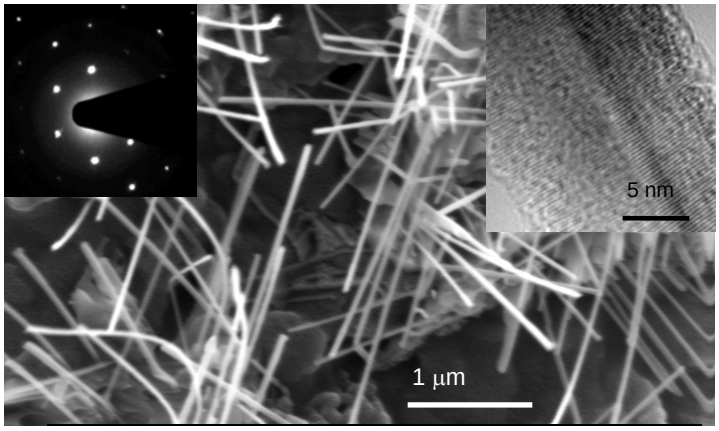

Figure 9. SEM of GaN:In nanowires on MCM-41 templates. Inset: High resolution TEM (right) and electron diffraction images (left)

The morphology of MOCVD-grown AlGaN nanowires with a varying vapor-phase Al content, $x_{Al\text{-}gas}$ = [TMAl]/([TMAl]+[TMGa]), is surveyed by SEM and summarized in Fig 10. Nanowires are observed in samples with Al vapor content from 30 to 90%. As the Al concentration is increased, an inverse dependence is observed between the length

of the wires and the density of the nanowires/nanocrystals. Samples with a high $x_{Al\text{-}gas}$ exhibit a clean background and a low density of long (4-5 μm) nanowires while samples with low $x_{Al\text{-}gas}$ are characterized by short, rod-like (1-2 μm) nanowires with nanocrystals decorating the background. Quantitative analysis of such morphological trends is hindered by a random, haystack distribution of nanowires on alumina substrates; details of the analysis of epitaxially aligned AlGaN wires on crystalline templates will be reported elsewhere. Under the same flow conditions with the same metalorganic flow rate, growth of GaN results in a mixture of short nanorods and nanocrystals while growth of AlN leads to a thin film coating that conforms to the morphology of alumina substrates under SEM imaging.

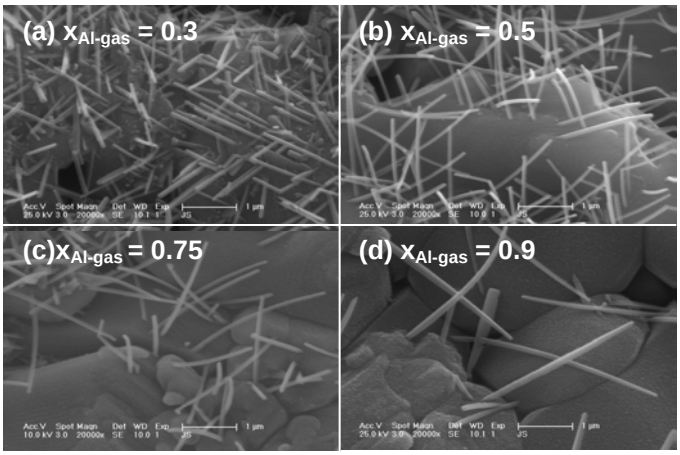

Fig 10. SEM images of AlGaN nanowires on alumina templates with Al gas phase ratio $x_{Al\text{-}gas}$ = 30%, 50%, 75%, and 90%

Microstructural analysis was carried out on nanowires that had been sonicated in solvent solution and dispersed onto TEM grids; a typical example is shown in Fig 2a. A contrast of dark inner core and light outer sheath is observed for all the AlGaN nanowires imaged. Thickness and the degree of tapering of the outer sheath region increases with the increase of $x_{Al\text{-}gas}$; a slope of ~11 nm/μm is estimated for the 90% sample. Chemical analysis by selective area EDS, with an electron-beam cross-section of 3nm in diameter, was performed at five different spots over the width of the nanowires. Normalized composition profiles based on Al and Ga line peak intensity ratios are shown in Fig 11b. The image contrast in Fig 11a correlates well with the composition profile (Fig. 11b) according to a designation of an Al-rich sheath region and a core consisting of primarily GaN. Our observation of spontaneous formation of coaxial AlGaN nanostructures resembles an earlier finding[29] of synthesis of AlGaN nanowires by a hot-wall furnace reactor in which a lattice mismatched strain was proposed as a driving force responsible for the formation of spatially segregated coaxial nanowires.

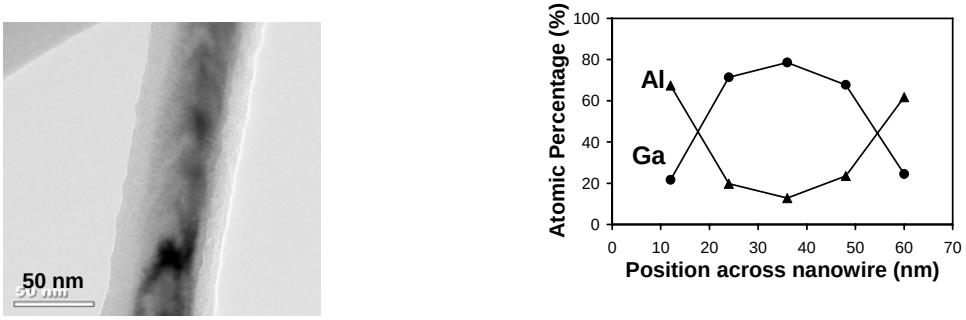

Figure 11. (a) TEM of AlGaN nanowires with $x_{Al\text{-}gas}$ = 50%, (b) Normalized composition profile across the nanowire Composition profile across the nanowire, the horizontal axis is the position across the nanowire, vertical axis is the atomic percentage of Al (triangular), Ga (round), and N (square).

Nanowire synthesis based on near-equilibrium vapor-liquid-solid (VLS) principle in flow-tube environment is a well-documented procedure.[30] Growth selectivity is derived from a preferential incorporation of vapor species through or around catalyst nanodroplets and a negligible growth rate at the vapor-solid interface imposed by minimum supersaturation near equilibrium. In the synthesis of nanowires using non-equilibrium, epitaxial techniques such as MOCVD and MBE, surface kinetics including adatom diffusion need to be taken into consideration.[31] It was shown recently[32] that growth of InAs nanowires using CBE takes place largely through the preferential incorporation at the droplet tip of adatoms that are within the radius of the diffusion length. In our attempt of synthesizing AlGaN nanowires by MOCVD, presence of both Al and Ga adatoms, as well a large difference in bond strength and consequently diffusion mobility between the two species,[33] creates a unique interplay between kinetic and thermodynamic processes which will be elaborated in the following.

Fig 12a shows a high resolution TEM image near the tip of a nanowire oriented in the [101-0] direction. For all the nanowire tips examined, the width of the core (GaN) region as determined by the contrast is well correlated with the physical dimension of catalyst droplets, suggesting strongly that the preferential incorporation into and the formation of GaN core region is linked to the catalytic growth. The presence of Al-rich Al(Ga)N outer sheath that is located outside the shadow projection of nanodroplets is unlikely related to catalytic growth. Observations of the absence in lateral over growth of AlGaN[34] and little surface diffusion of Al adatoms lend credibility to a model that the AlGaN outer sheath is deposited through conventional vapor-solid growth with negligible selectivity. Such a designation provides an explanation of the increased tapering of AlGaN nanowires with an increasing $x_{Al\text{-}gas}$ since the tapering slope represents an indicator of the prevalence of sidewall growth. We note that the dimensional matching between catalyst nanodroplets and the core diameter of coaxial nanowires has been reported in the intentional overgrowth of InGaN shell on pre-grown GaN nanowires.[35]

High-resolution TEM also reveals the presence of well-defined crystallographic planes at the nanowire tips that can be categorized into inclined (Fig. 12a) and pointed (not shown) for [101-0] and [112-0] nanowires, respectively. Crystallographic analysis on both types nanowires indicate the droplet/nanowire interfaces in both cases correspond to pyramidal [101-1] plane, a plane that is likely to have the lowest surface energy or growth rate during the MOCVD growth of GaN.[36] Based on the electron diffraction data, crystallographic symmetry, and ELO works, a three-dimensional reconstruction of the tip

structure is given in Fig. 12b. Shape evolution in nucleation and nanocrystal growth has been analyzed by Wulff theorem in terms of surface energy and adopted to the kinetic consideration of growth rates. [37] A well-known phenomenon is that a rapidly growing surface (or thermodynamically a crystal facet with high surface energy) tends to grow itself into extinction. Our consideration of surface energetics (Fig 12b), on the contrary, leads to an intriguing if not paradoxical distinction for nanowire growth in which selective and preferential growth, mediated by the presence of catalyst and/or liquid droplets, takes place at and is confined to a surface/interface with a low surface energy,[38] thus forming a self-sustaining growth process.

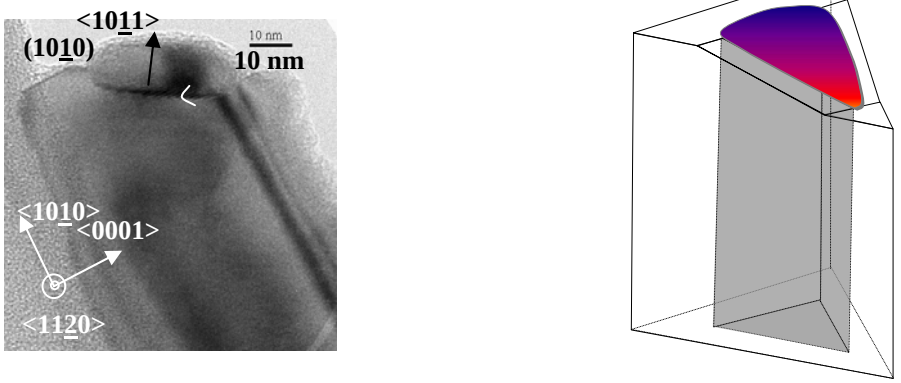

Figure 12. (a) HRTEM of AlGaN ($x_{Al\text{-}gas}$ = 50%) nanowires near the tip region, the nanowires growth direction is along <10$\bar{1}$0> and the view angel is parallel to (10$\bar{1}$0) plane and along<11$\bar{2}$0> direction, with a very small degree of tilting toward <0001> or <000$\bar{1}$> direction, (b) 3D diagram of the TEM image, the triangular cross section is bound by two {11$\bar{2}$2} planes and basal (000$\bar{1}$) plane, the droplet is on the tilted (10$\bar{1}$1) plane.

To ascertain both the optical quality and the spatial distribution of the alloyed nanostructures, catholuminescence was performed on two samples with $x_{Al\text{-}gas}$ =50% and 70%. Fig 13a shows wide-area ($10\times10\mu m^2$) integrated scanning CL spectra in which emission from both samples are dominated by a broadened GaN band-to-band recombination peak at 370nm at 105 K. A broad shoulder on the high-energy side (~320 nm) is also observed in both samples. Origin of different emission signatures is investigated through monochromatic scanning CL mapping at a wavelength of 370 nm (Fig 13c) and 320 nm (Fig 13d), with SEM imaging recorded for spatial reference (Fig 13b). A point-to-point match between the nanowire features under SEM (Fig. 13b) and the spatially resolved emission pattern at 370 nm (Fig. 13c) unambiguously associates the dominant GaN emission to the individual nanowires, presumably from the core region of the coaxial AlGaN nanowires. Furthermore, CL mapping at 320 nm reveals a nearly homogeneous distribution of AlGaN, consistent with the notion that, under the growth condition employed; Al has a relatively low surface mobility.

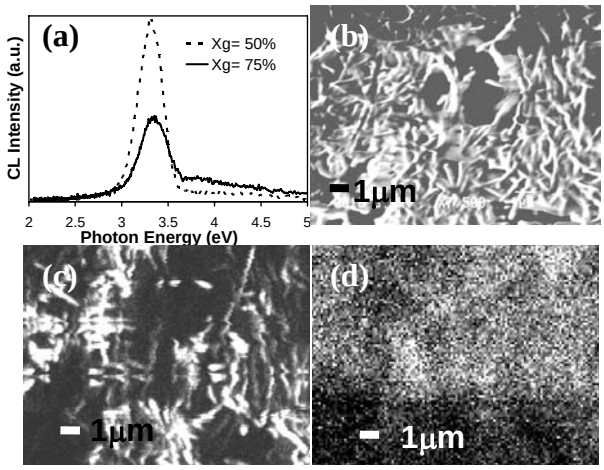

Figure 13. (a) Wide area (10×10 μm^2) integrated scanning CL spectra at 105 K for AlGaN nanowires with $x_{Al\text{-}gas}$ = 50% and 75%, (b) SEM image of AlGaN nanowires with $x_{Al\text{-}gas}$ = 75% on alumina substrate, (c) monochromatic CL map of the same area at wavelengths of 370 nm (3.35 eV), (d) monochromatic CL map of the same area at 320 nm (3.87 eV). The scale bar is 1 μm. The white area corresponds to the position where CL intensity is strong.

Non-equilibrium growth processes such MOCVD and MBE have been instrumental in preparing ternary and quaternary semiconductors in planar epitaxy. Attempts to produce nano-planar, patterned growth of alloys often results in complex composition profiles due to disparate and competitive kinetic properties among the constituting elements. The spontaneous formation of coaxial AlGaN nanowires through conventional procedure of precursor mixing in a MOCVD process attests to the complicate nature of non-equilibrium growth. In addition to the catalytic growth of GaN core and the V-S deposition of AlN sheath, we note that the concurrent presence of Al adatoms (or AlN) leads to a surprising phenomenon of enhanced surface diffusion of Ga adatoms, as can be inferred from Fig 1 with a reducing density and increasing length of nanowires as $x_{Al\text{-}gas}$ increases. This hypothesis is corroborated by a report that AlN is effective as a mask in epitaxial lateral over growth,[39] indicating that the diffusion of Ga adatoms on AlN (or high Al containing alloy) is greatly enhanced. It has been pointed out that engineering of surface energy play a crucial role in controlling the shape and morphology of nanostructures.[40] In the synthesis of AlGaN nanowires, it is speculated that the passivation of the GaN core by the AlN sheath helps to stabilize the sidewall facets and improve the nanowire viability at nucleation stage, bearing the same root as earlier reports using hydrogen or oxide.

Growth of patterned GaN nanowires: We have shown in previous months the plausibility of forming arrays of GaN nanorods, which are promising nanostructures as the medium for light emission and light extraction. In the month of January we explored the possibility of combining patterned wafers, through epitaxial lateral overgrowth (ELO), with aligned nanowire growth in order to achieve interconnected nanowire structures. Fig 14 shows GaN nanowires (running horizontally) that are interconnecting the hexagonal GaN mesas formed by ELO. (The hexagonal spatial distribution is arranged through photolithography.) The horizontal arrangement of GaN nanowires could potentially increase the surface area and further the external quantum efficiency.

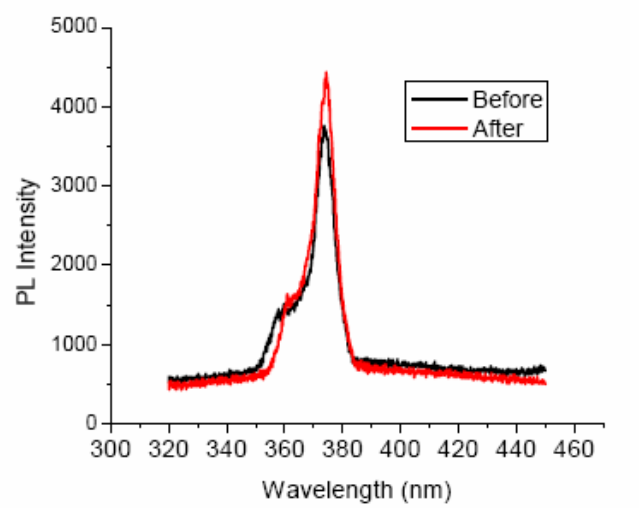

Fig 14. Room temperature PL emission spectrum GaN nanowires (black trace) and "InGaN-GaN" nanowires.

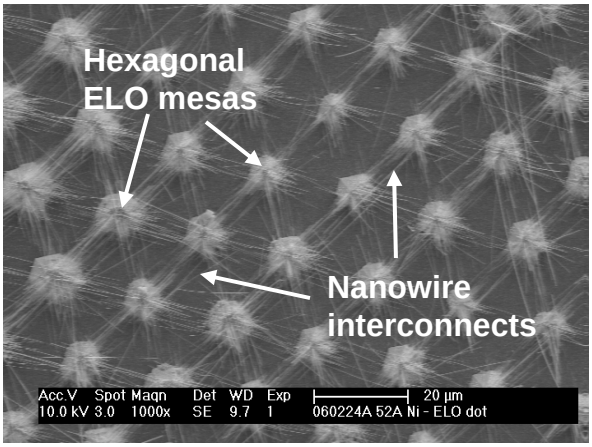

Fig 15 Top view SEM of nanowire interconnected networks

III.E AlN/GaN DBR mirror with R>95%

The large number of AlGaN/GaN layer pairs (>50) to achieve the high reflectivities present sizable difficulties in the control of cracks and the DBR morphology. It has been discovered recently[41,42] that the use of AlGaN interlayers is effective in controlling mismatch-induced stress and suppressing the formation of cracks otherwise occurred during growth of AlGaN directly upon GaN epilayers. During the first year we have completed the growth and calibration of epitaxial AlGaN/GaN distributed Bragg reflectors (DBR) toward the fabrication of 410 nm vertical cavity emitters for enhanced spontaneous emission and light extraction. Important issues related to the DBR growth include 1) Morphological control at macroscopic (mm-scale) and atomistic levels, both are related to the morphology of starting GaN templates, 2) Control of mismatch strain through the use of interlayers or supperlattices, and 3) N-type doping to enable current injection through the mirror. We achieved in this year the growth of 20-pair AlGaN (35%)/GaN DBRs with good morphology (under Nomarski microscope as well as AFM) and tunable reflectance peak from 390 nm (Figure 16) to 440 nm (not shown) by changing the periodicity of the DBR layers. A 90% peak reflectance and stop bandwidth of almost 20 nm have been achieved. The use of stress-control AlN interlayer helps to eliminate all the crackings. It is our opinion that the epitaxial DBR mirror has reached a level that can support serious VCSEL pursuit.

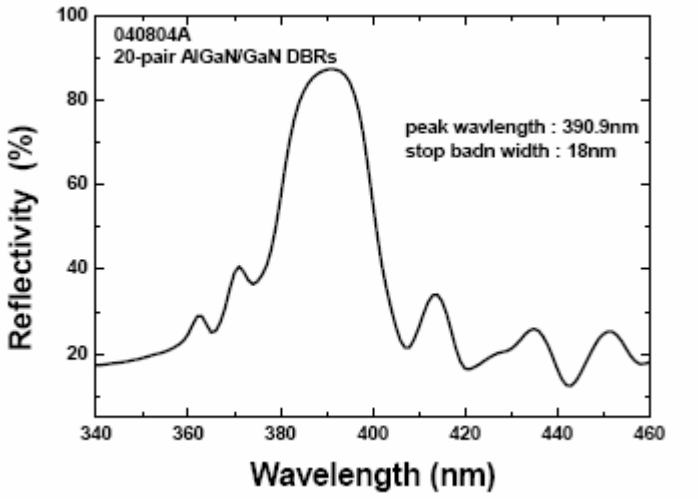

Fig 16. Reflectivity of AlGaN/GaN distributed Bragg reflector with 20 pairs and a periodicity of 74 nm.

III.F Nano ELO and Selective Area Epitaxy

Silicon dioxide masks (~70nm) were deposited on AlGaN epilayer, upon which nanometer-size windows with varying sizes and densities were patterned through e-beam

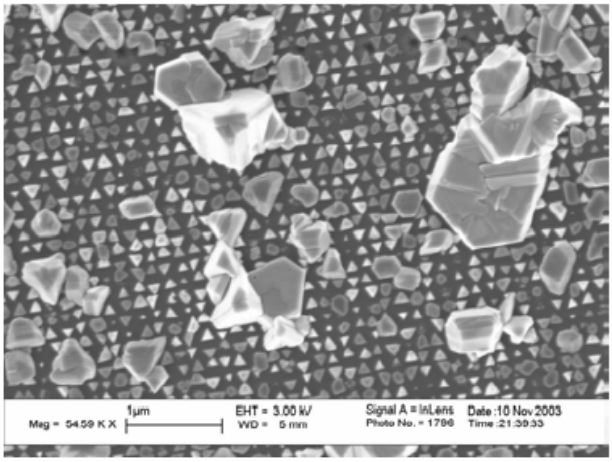

Fig 17. Nanoscale selective area growth (SAG) unveiling preferred orientations of lateral growth.

lithography. Re-growth was performed that consisted of three InGaN MQWs at low temperature followed by HT GaN growth. This growth serves to establish the baseline of the ELO growth condition. The triangular shapes of SAG mesas suggest the anisotropy in surface energy due to surface atomic arrangements.

III.G Photonic Crystal

In Section III.A we addressed experimental observation of enhanced and stimulated optically pumped blue emission from unique InGaN quantum well nanostructures, formed from planar LED-type wafers by electron beam lithography. The process resulted in ~60-90nm diameter nitride rods, densely arrayed with ~30 nm edge-to-edge inter-rod separation. We consider here possible photonic bandgap contributions to the observed low-threshold stimulated emission, formed due the periodic distribution of the refractive index. We have used simulation based on two dimension finite difference time domain approach (FDTD) to calculate the photonic bandgap element of our nanopost arrays. Figure 18 shows an example of the simulations of the photonic crystal structure, while Figure 19 displays the corresponding reflection spectrum in the spectral range of interest. We chose the input parameters as the follows: the GaN nano-post refractive index is 2.54, the nano-post diameter is 70nm, and the period of the nano-posts is 90nm. There is only a very narrow photonic bandgap near the QW emission (400nm), which means the photonic bandgap effect could be very weak. The reflection simulation is done with a launch of light from the edge of the nano-posts (2D), and the result shows that QW emission is at the edge of the photonic bandgap, i.e. at edge of the wavelength range where the light propagation is forbidden. It is also over what wavelength range of the photons that are confined and therefore feedback is provided. We need to point out the parameter values for inputs to the simulation are only the best

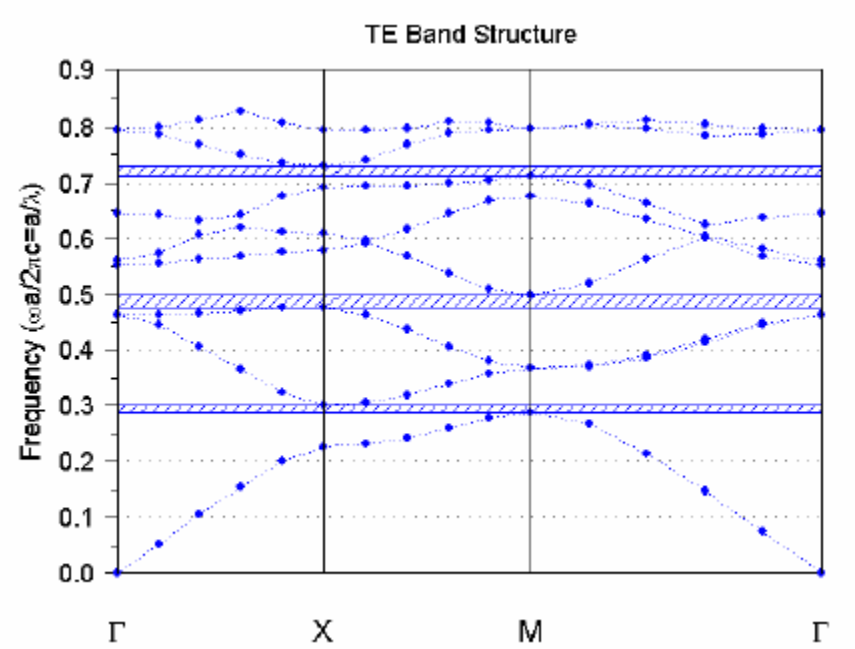

Fig. 18. Example of FDTD simulation of 2D photonic crystal structure for an array of 70 nm diameter InGaN QW nanoposts.

guess based on our knowledge. For example, the exact number of nano-posts' refractive index at high pumping levels is unknown. Another uncertainty is the diameter of GaN nano-posts. It is very hard to measure it accurately via SEM image due to the well-known charging effect in SEM. Unfortunately, our simulations show that the position of photonic bandgap is very sensitive to those inputs. So far, our experimental results could not totally rule out photonic bandgap lasing possibility. However, we need to point out that a difference between our device and a typical photonic bandgap laser is that our heterostructures do not have a designed waveguide for lateral propagation.

If the effect of photonic bandgap is indeed small, the stimulated emission we have observed could be the result of near field interaction between the nearest individual nano-size light emitters since, our nano-posts are so dense that the separation is below 30nm. In principle, the emission cross section of individual nano-post could be enhanced with such a close separation. To further study this effect, we have measured the carrier life-time at different pumping levels in spontaneous regime. We have observed that the carrier life-time decrease at higher pumping level. This result is opposite to a typical result for spontaneous emission, where the carrier life-time would increase due to the saturation of nonradiative recombination at high pumping level. At this point, we cannot not totally rule out the contribution by photonic bandgap effect to stimulated emission. However, the unusual optical effects seen in the laboratory, especially the spatially localized stimulated emission and carrier life-time results suggest that the stimulated emission is different from the stimulated emission which occurs in the presence of feedback from optical resonators.

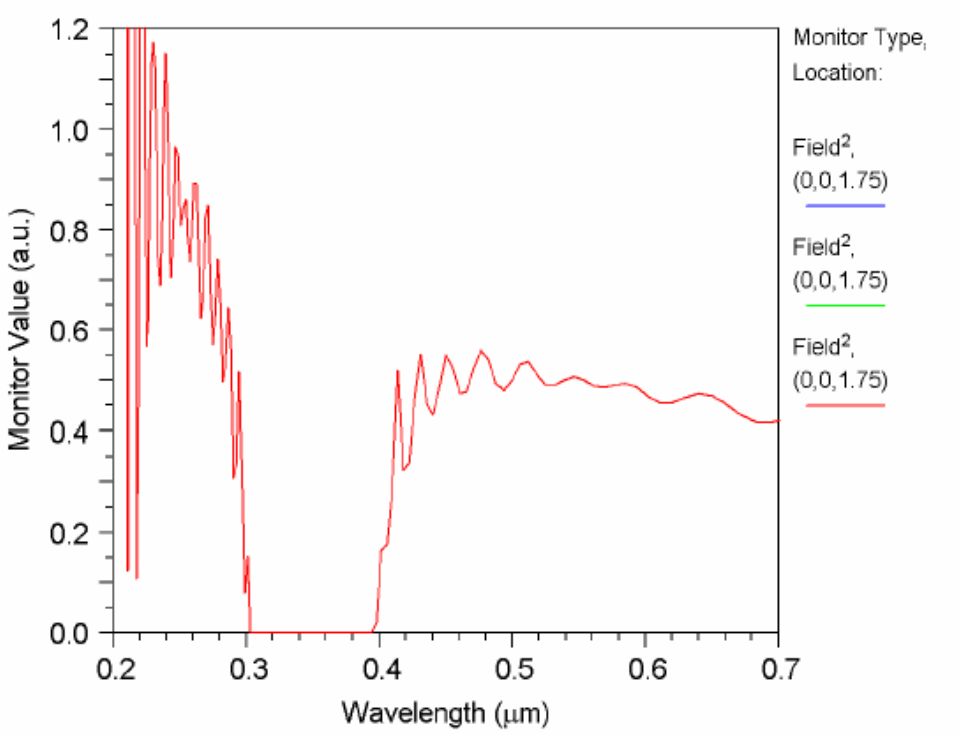

Fig 19 Effect of photonic bandgap in the near-UV range.

III.H Nanostructured light emitting medium: Superluminescence and Co-operative Radiative Effects

The nanotextured active media for high performance LEDs, which has been described in previous sections as quantum dots or nanowires, is ultimately aimed to forme very high density arrays e.g. from InGaN nanorods. In this contract we have explored a new physical idea, namely that a high density ordered spatial assembly of these sub-wavelength sized elements forms strongly coupled highly proximate coupled arrays of photonic elements as the basis of the new active photonic media. The innovation in and potential advantages of this type of solid-state lighting media can be summarized as follows: (1) the efficiency of light emission is enhanced because of lateral photon localization and because the photon escape from the arrays is governed by light scattering, not by total internal reflection; (2) the nanorods and nanotubes have such a small individual physical volume that extended defect (dislocation) formation is unlikely, thereby in principle eliminating a deleterious nonradiative recombination pathway. Finally, (3) at small nanorod spacings (<50 nm) the spontabeous emission rate can in principle further accelerated because of the dipolar coupling of nearest neighbor emissive nanorod excitonic "antennae" (in analog to Forster coupling, or photon tunneling in molecukar media).

In comparison with other approaches to patterned active light emitting media, we emphasize that the regime of optical and optoelectronic response of interest here lies ***below*** the size regime for photonic crystals, making our nanorod arrays especially fault intolerant in terms of the strict periodicity required from photonic crystals. In particular,

we will employ nitride nanowire and coaxial nanotube arrays such as shown in Fig. 15, which are 'automatically' highly dense and ordered by the synthesis techniques which exploit the epitaxial VLS growth method and described in the next section.

As a demonstration of the new types of light emitting qualities of InGaN-based 'nanorod ensembles' for enhanced light emission response, we have employed "top-down" approach at Brown (Nurmikko) via electron beam lithography and specialized chemical etching as a fabrication approach. While this approach to nanotexturing is impractical for large volume manufacturing (as opposed to the bottom-up approach emphasized above) individual nanopost diameters on the 50 nm scale can be achieved to craft the arrays to reach a henceforth largely unexplored regime with high density arrays, where in-plane photon localization and ease of photon escape are anticipated, with adjacent InGaN dipolar optical elements placed within a few tens of nm of their nearest neighbors. Figure 20 shows scanning electron beam microscope images of one high-density square array at two different levels of magnification. Macroscopic array sizes up to about 60μm x60μm were fabricated. Earlier research has suggested that ***nonradiative*** recombination at free surfaces of GaN and its alloys does not dominate electron-hole pair dynamics to the same degree of severity as with 'conventional' III-V semiconductors. This seminal behavior appears to be a combination of the innate ability of the nitride surfaces to reconstruct so as to remove the surface Fermi level from the bandgap, and the short e-h diffusion lengths due to carrier localization in InGaN QWs (from pronounced alloy potential fluctuations). Here we are able to infer such a conclusion quite directly by employing the very small laterally patterned structures with their large surface-to-volume ratio, where the free surfaces have been prepared by a dry etching process that involves both chemical and physical factors in exposing the QW (and adjacent GaN sidewalls) to free space. Our data of relative luminescence efficiency and lifetime measurements (from transient photoluminescence) suggests that radiative recombination remains the dominant process for the e-h pairs in the patterned nanopost samples.

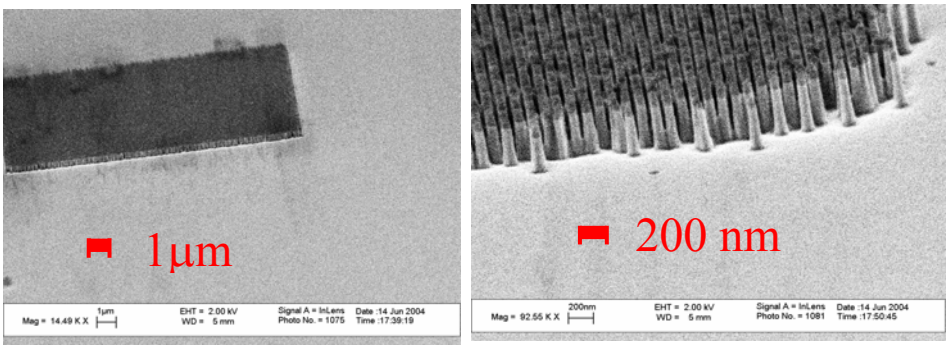

Figure 20. *(a) Global view of patterned InGaN MQW nanoposts; (b) Image under higher magnification of 60nm diameter nanoposts with 30nm edge-to-edge separation.*

We have discovered in our recent work that, remarkably, the dense InGaN/GaN MQW square nanopost arrays in the violet, such as in Fig. 16, also readily demonstrate a propensity for stimulated emission (or "superluminescence") under modest optical excitation conditions. Figure 21 shows the emission spectrum near 400 nm, acquired by

optical pumping of a nanopost array over a micrometer scale lateral area. Closer examination under high resolution microscopy has indicated that stimulated emission occurs in "local neighborhoods" that appear to involve small clusters of nanoposts, within which photons in the lateral (layer) plane are recycled and amplified. At one level, the heterogeneous nanoscale material, with strong light wave scattering, induced by the sub-wavelength structure, can provide for such photon localization which in the presence of high gain can be envisioned to lead to an effective local feedback, i.e. structurally enlarging the effective local dipole moment. Such in-plane photon localization reduces the self-absorption and, more importantly, gives rise to efficient photon escape from the material. We emphasize that the size and density range of the nanopost arrays is such that conventilnal photonic crystal effects are not dominant. Rather, we have in these laterally localized modes a parallel to localized wavefunctions in disordered solids. In the regime of high density periodic "tight" array of nanoposts, the in-plane light scattering acquires also an additional coherent backscattering component [Ref XX]. Figure 18 shows how the spatial architecture of the nanorod arrays affects the polarization characteristics of emission, here in case of linear arrays of nanoposts.

By using high resolution near field scanning optical microscope (NSOM), we are currently investigating the details of the photon localization in terms of the local in-plane confinement and light extraction. Figure 21 shows two examples of NSOM images, taken perpendicular to the sample plane for a linear array of nanoposts (left panel) and from a square (2D) array (right panel), respectively. In each case the arrays have significant fabrication related discorder in terms of the regularity of the nanopost spacing. Our NSOM has approximately 80 nm spatial resolution at the moment but nevertheless reveals clearly enhanced light emission from local "hot spots". When comparing these hot spots with corresponding AF< topographical images (not shown here), we conclude tentatively that these spots correspond to neighborhoods where nanorod features are more precisely formed than at other locations.

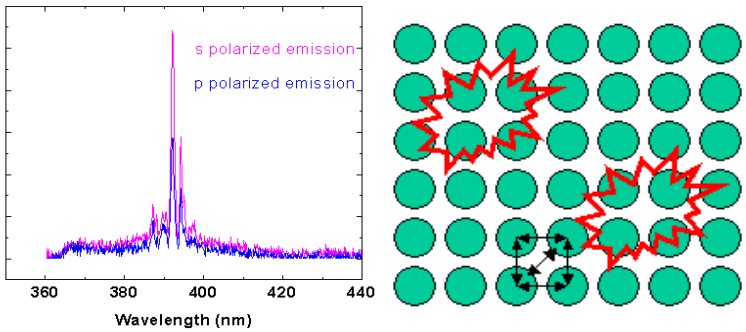

Figure 21. *(left) Stimulated emission from InGaN "superluminescence"; (right) cartoon illustrating the photon localization and emission enhancement concept in nanotextured media.*

Another fundamental and exciting physical mechanism, beyond simple photon localization and by "photon recycling", arises from the physics of light-matter-interaction of this type of nanoscale nitride composite due to near-field dipole-dipole interaction (photon tunneling) between adjacent nanocrystal elements. In molecular systems, this coupling is the Forster transfer (FRET) which scales as R^{-6} with the separation between

the adjacent chromophore sites (assumed as point sources in 3D), and is typically effective for R<10nm. In case of excitons in the InGaN system, given their large oscillator strength (i.e. effective dipole moment > 1Debye), we have estimated that Forster effects should become effective at interpost separation on the order of 50 nm. If coherent, the process can produce a giant (dipolar) oscillator strength associated for both light absorption and emission, concentrated within a designed spectral bandwidth. Such collective excitonic enhancements will be of importance in endowing nanoparticle arrays further optoelectronic prowess not available in other types of patterned nitride semiconductor materials (e.g. photonic crystals).

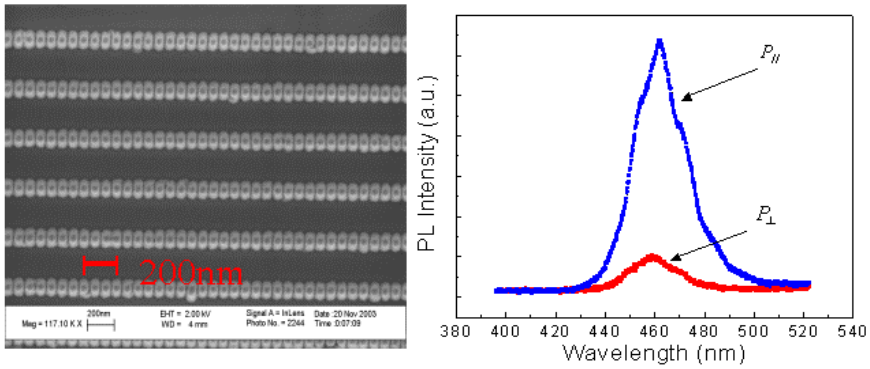

Figure 22. *(a) Electron microscope top view of linear InGaN nanopost arrays C. (b) Polarized spontaneous emission from such arrays, demonstrating clear emission anisotropy.*

III.I Hybrid Organic-Inorganic light emitting medium for green LEDs

Since January 2006 we began to consider a new type of LED structure including a conventional InGaN quantum well emitting at purple or blue (400-450nm) that is placed *in close proximity* to an organic thin layer (poly (p-phenylenevinylene), PPV, for example). The close proximity between the inorganic and organic layer can facilitate an efficient energy transfer mechanism (Förster resonant energy transfer, FRET) to transfer the electrically injected carriers, which are funneled into and localized within the InGaN quantum well, into the adjacent polymer layers. An important design consideration is the spectral overlap between the emission peak of the exciton donor layer (InGaN) and the absorption peak of the exciton acceptor layer (PPV). The idea of FRET-based enhancement is provided in Fig. 23.

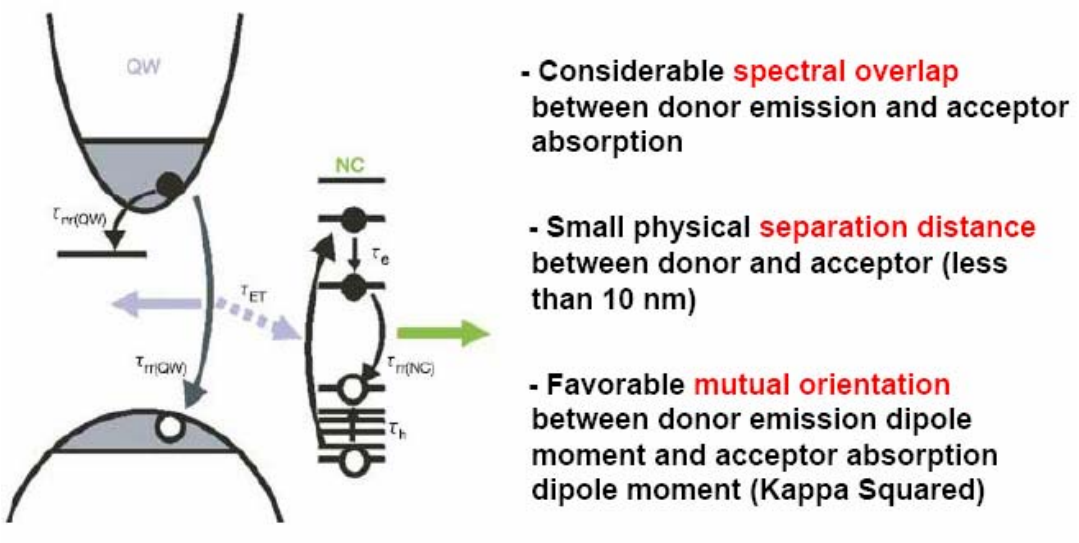

Fig 23. Schematics showing the competition between radiative, non-radiative, and FRET processes in an organic/inorganic hybrid structure.

We reported the investigationof hybrid LED structures using n-type InGaN with PPV polymer prepared by CVD. This month we began the investigation the use of spin-coating to apply blue-polymer, Poly [9,9-di-(2' ethyl-hexyl) fluorenyl-2, 7-diyl], and green polymer, Poly [9, 9-(2'-ethylhexyl)-9H-fluorene-2, 7-diyl], to a variety of semiconductor surface.
Preliminary results showed that the two PPV derivatives produce the desirable emission wavelength. The use chrolobenzene leads to a thicker polymer film than that from toluene solution. Spin rate is adjusted between 3000 to 8000 rpm, leading to thin films of thickness between 0.2 to 1.0 μm. Initial PL results reveal possible enhancement in the emission efficiency from the organic thin film even though sample uniformity and degradation emerge as a main concern. We have identified the potential recombination, energy transfer, and carrier transport pathways and will design experiments to elucidate and clarify the origin and plausibility of FRET-based devices.

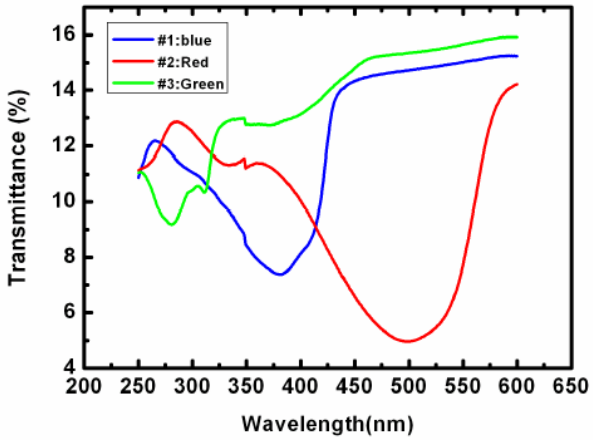

Fig 24. Transmittance of blue, green, and red polymers on sapphire showing strong absorptions at 380, 400, and 500 nm, respectively..

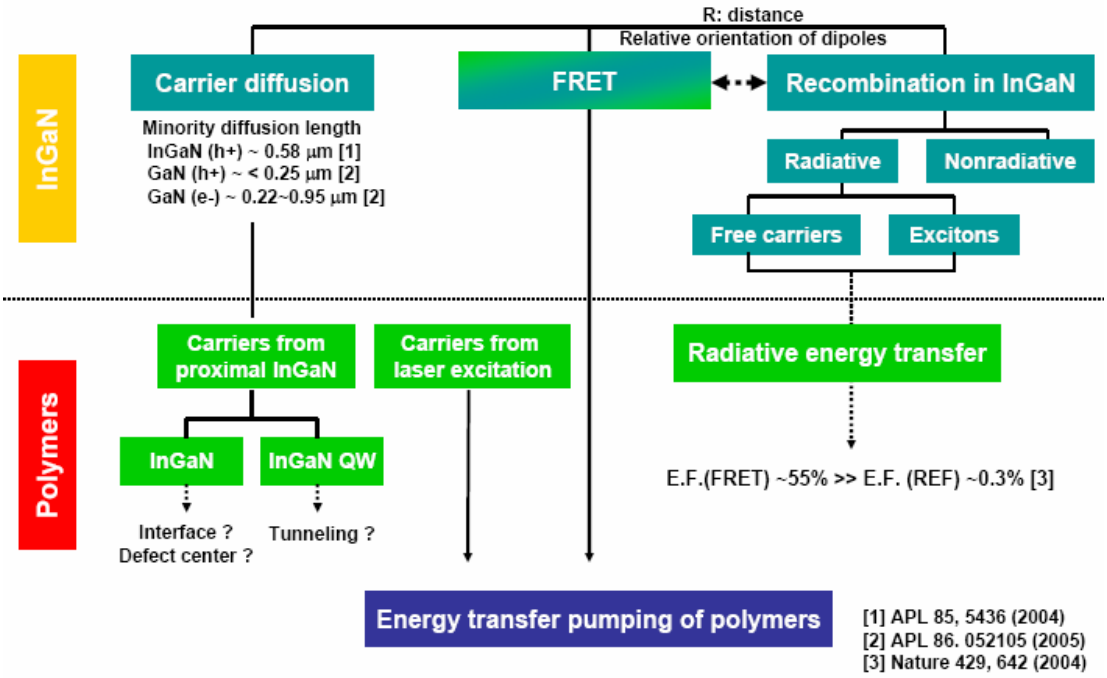

Fig. 25 Carrier transport mechanisms across the hybrid interfaces.

With active push to improve performance and extend the application range of InGaN-based devices in solid state lighting, as well as reaching into areas such as photovoltaics, new exploration space includes nitride nanostructures and integration of non-nitride materials within active devices. For example, one key challenge with nanostructured (or "nanotextured") heterogeneous nanostructures such as high density arrays of InGaN crystalline nanowires is the implementation of electrical interfaces, where an electronic interface with soft organic semiconductors can be useful. With these opportunities in mind, we have investigated planar heterojunction structures composed of various layered arrangements of various small organic (electron/hole transport) molecules atop n- and p-type GaN/InGaN heterostructures, to gain insight into the details of electronic nature and charge transport across these "hybrid" inorganic-organic semiconductor structures. While crystalline inorganic and organic semiconductor junction devices are generally viewed as distinct and separate technologies, few examples of mixing two such disparate electronic materials exist. Earlier work e.g. by Hyunh et al has shown charge transfer between colloidal II-VI nanocrystals immersed within an organic conducting polymer matrix, while Coe et al fabricated an LED where II-VI nanocrystals were imbedded within a planar organic junction.

We have recently studied planar heterojunctions, based on an n-type GaN or InGaN/GaN QW single crystal epitaxial layer (Si doped, n ~ $1x10^{18}$ cm^{-3}), onto which thin films (<100nm) of about a half a dozen different were deposited (such as Alq_3 , BCP, and α-NPD, typical in organic LEDs). These structures showed good charge transport across the (presumably Van de Waals bonded) organic-inorganic hererojunctions, highlighting the relative ease of hole transport from organic to the n-GaN layers.

In this work, we have employed an InGaN/GaN blue LED material as the template and deposited different organic thin films as part of the hole injector circuit in such a hybrid device. In standard practice of blue and green LED fabrication, securing ohmic contacts to the topmost p-GaN layer requires careful metallization and thermal annealing steps, which can be constrictive to the overall device device processing or architectural innovations. We show here just one example of our extended studies (I-V characteristics, light emission spectra, photovoltaic response, and AFM/NSOM morphology work)), namely of an Au/α-NPD/p-GaN/InGaNQW/n-GaN heterojunction blue light emitter. **Figure 26** shows the schematic of the device structure, together with possible electronic state alignments based on electron affinity data at zero bias without interface charge etc. The organic semiconductor α-NPD is typically used as a hole transport layer in all-organic LEDs but, depending on the energetic relationship (i.e. "bandoffsets) between the conduction-valence bands of the nitride and the HOMO-LUMO gap of the organic, may transport holes as well. **Figure 27** shows the room temperature current-voltage and light emission characteristics (L-I-V) of one planar hybrid device at room temperature, with the I-V compared with a standard all-inorganic device made from same nitride material without the organic thin film. The figure also shows spectrum of the hybrid blue LED and the homogeneous light distribution across a large area device. The spectrum is dominated by the emission from the InGaN QWs, with a broad spectral contribution from the so-called GaN buffer layer yellow luminescence. However, we also see emission from the organic layer near 450 nm, whose magnitude depends on many device design and operational conditions. It is important to notice that the hole injection through the organic layer appears to be quite effective and practical in enabling a high brightness blue InGaN QW LED. Moreover, the current densities employed here exceed significantly those which are possible in all-organic LEDs. The mechanism of injection and the electroluminescence characteristics depend on the particular combination of the nitride and organic thin films, suggesting that our hybrid system has potentially considerable versatility in the design and tailoring of specific charge transport and optical properties in novel

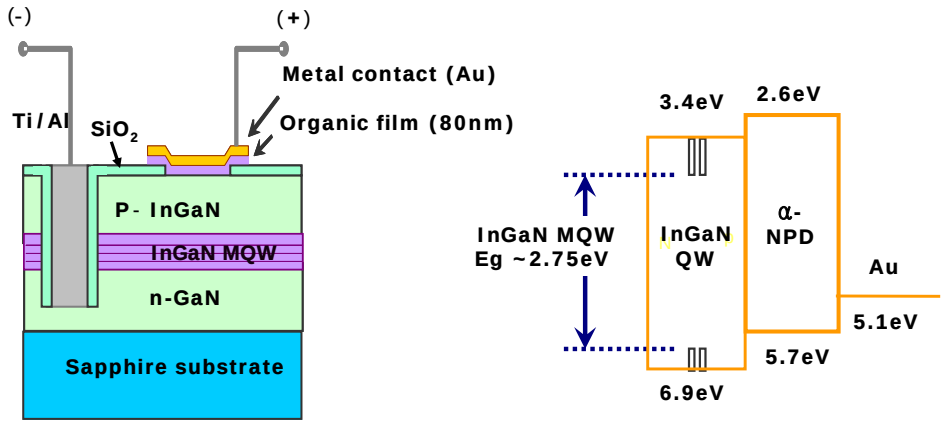

Figure 26: (Left) A InGaN QW pn junction nitride-organic heterojunction device geometry, incorporating a 80 nm thick organic (α-NPD) layer as part of the hole injection structure. (Right) Zero-bias electron affinity hypothetical electronic state lineup at organic/nitride junction

LEDs which draw usefully from the hybrid material concept.

We report on the advances made in developing a p-contact alternative for hole injection into InGaN MQW based blue and green LEDs. The strategy is based on the use of a thin organic layer as the hole transport layer to the topmost p+-GaN layer. Since the evaporation of the organic layer can be accomplished at near room temperature and the thin film is mechanically flexible, this approach can offer new opportunities in configuring LED as high density arrays as well as wide area nitride illumination sources.

As indicated in our last report, we have focused on the use of small molecule organic semiconductors to study the charge transport across interfaces between GaN and the organics. Of a wide range of organic semiconductors tested, we have had recent success with α-NPD, an organic semiconductor which is used as a hole transport layer in all-organic LEDs. As the base device material, we have employed a standard blue LED InGaN QW wafer material on top of which, after thorough surface cleaning, <100 nm layer of α-NPD and a thin Au electrode film are deposited by ultrahigh vacuum evaporation equipment. These deposition steps occur at room temperature and are thus simpler than the conventional Ni/Au (or other alloying schemes) for p-contacts which require a careful high temperature annealing step.

The basic device test structure employed by us is shown in Fig. 26(a), where the n-contact to the n-GaN epilayer is fabricated by standard techniques, but the p-contact is replaced by the organic thin film injector. Fig. 26(b) shows the corresponding emission spectrum of this inorganic-organic hybrid LED device at three different levels of voltage bias.

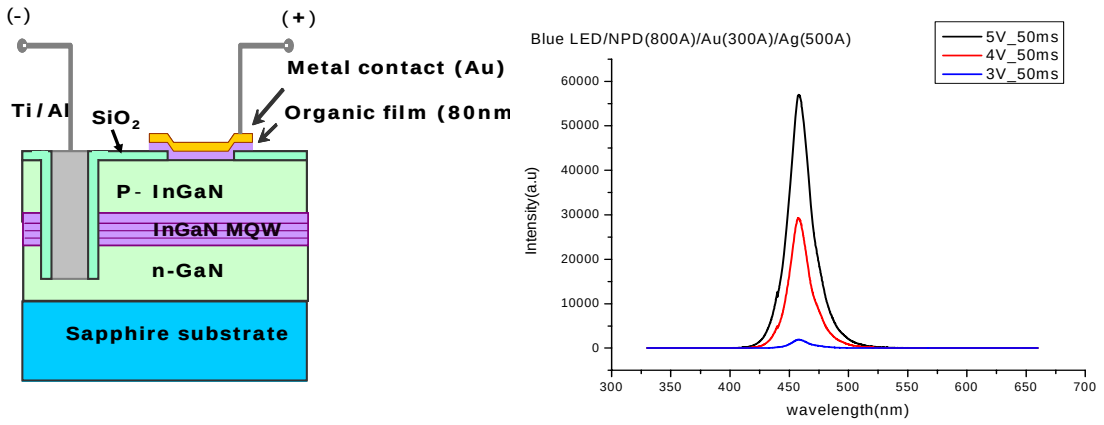

Figure 18: (a) InGaN blue LED with organic hole injector, (b) emission spectrum from the QW device

The current-voltage and light output power vs. voltage are shown in Fig.27 for an approximately (600 μm)^2 inorganic-organic hybrid device. When compared with the

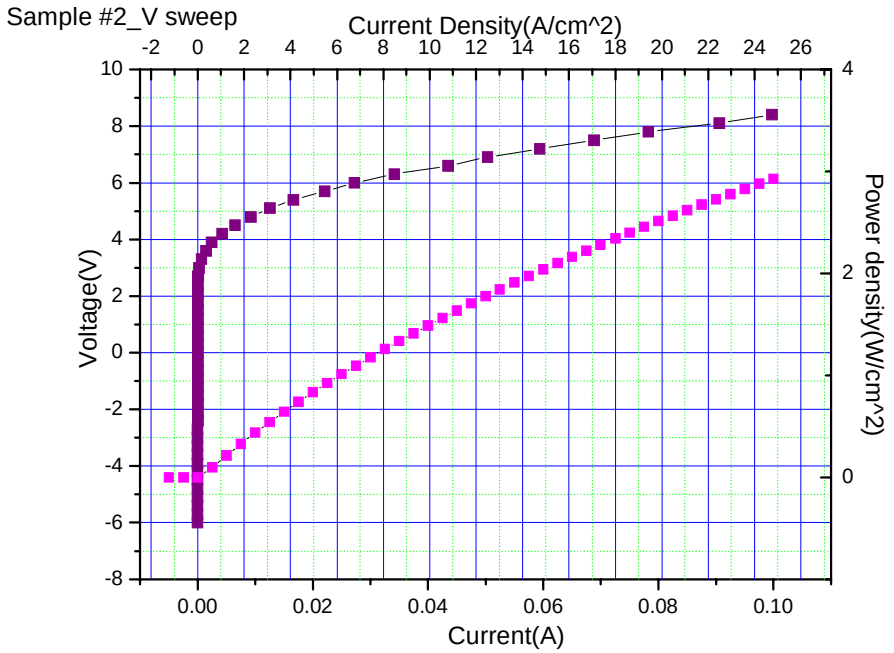

Figure 27: LIV performance curves of a InGaN QW blue LED with organic hole injector layer.

performance of devices from the same wafer with conventional high-T processed p-contacts, the extra overhead in terms of voltage drop across the organic layer is at most 0.5 V in these (so far) unoptimized first devices. Also note that the current density employed is in an acceptable range for a blue (or white) nitride LED, while exceeding significantly those for all-inorganic LEDs. Ongoing work is now focused on understanding the microscopi details of charge transport of holes across the organic/p-GaN heterointerface.

Since January 2006 we began to consider a new type of LED structure including a conventional InGaN quantum well emitting at purple or blue (400-450nm) that is placed *in close proximity* to an organic thin layer (poly (p-phenylenevinylene), PPV, for example). The close proximity between the inorganic and organic layer can facilitate an efficient energy transfer mechanism (Förster resonant energy transfer, FRET) to transfer the electrically injected carriers, which are funneled into and localized within the InGaN quantum well, into the adjacent polymer layers. An important design consideration is the spectral overlap between the emission peak of the exciton donor layer (InGaN) and the absorption peak of the exciton acceptor layer (PPV).

We reported the investigationof hybrid LED structures using n-type InGaN with PPV polymer prepared by CVD. Additionally we have carried out an investigation the use of spin-coating to apply blue-polymer, Poly [9,9-di-(2' ethyl-hexyl) fluorenyl-2, 7-diyl], and green polymer, Poly [9, 9-(2'-ethylhexyl)-9H-fluorene-2, 7-diyl], to a variety of semiconductor surface. The use chrolobenzene leads to a thicker polymer film than that from toluene solution. Spin rate is adjusted between 3000 to 8000 rpm, leading to thin

films of thickness between 0.2 to 1.0 μm. Preliminary results showed that the two PPV derivatives produce the desirable emission wavelength.

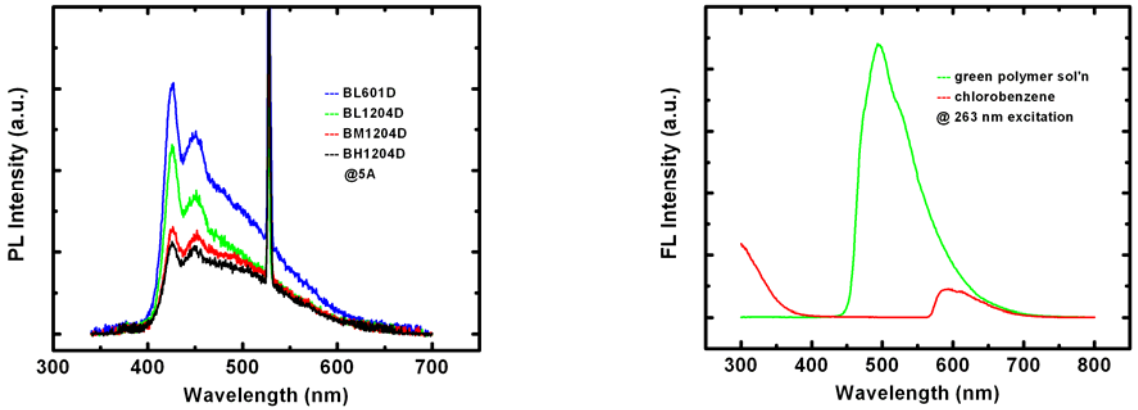

Fig 29. (Left) PL of blue polymer that was spin-coated on silicon wafer, and (right) PL of the green polymer that is in chlorobenzene solution.

IV MILESTONE SUMMARY

- Synthesize 410 nm light emitting medium with Internal Efficiency ~1.0
  Status: Achieving ~30% (determined by temperature-dependent PL)

- GaN Dots ~370 nm Internal Efficiency ~.8
  Status: NYR*

- GaN Wires ~370 nm Internal Efficiency ~.8
  Status: Achieving 10% determined by CL

- AlN/GaN DBR Mirror w/R>95%.
  Status: Demonstrated 99% reflectivity at 380 nm

- Nano ELO and SAE Internal Efficiency ~.8
  Status: NYR

- Photonic Crystal External Efficiency ~.5
  Status: Observed up to 5 times improvement in light extraction

- GaN/air DBR Mirror w/R>95%
  Status: Project redirected due to difficulty in PEC etch (revised in 2005)

- Microcavity Extraction Efficiency ~.5
  Status: Emission directionality was confirmed

- Superluminescent Medium Internal Efficiency
  Status: Approaching ~100% (determined by temperature-dependent PL)

- Design/Create High-Q Low Loss Resonator
  Status: Accomplished (quality factor > 600)

*Not yet reached.

V LIST OF PUBLICATIONS AND PRESENTATIONS

Presentations

- J. Han, "III-N Exploratory Devices and Nanostructures", seminar at Princeton University, May 2004.
- J. Han, "III-N Exploratory Devices and Nanostructures", seminar at Paul Drude Institute, Berlin, Germany, May 2004.
- J. Han, "III-N Exploratory Devices and Nanostructures", seminar at EPFL, Lausanne, Switzerland, May, 2004.
- M. Gherasimova et al, "Fabrication of GaN Quantum Dots on AlGaN Template by Liquid Droplet Epitaxy", presented at EMC, Notre Dame, Indiana, June, 2004
- J. Su et al, "MOCVD Growth and Characterization of GaN nanowires", presented at EMC, Notre Dame, Indiana, June, 2004.
- M. Gherasimova et al, A nanocluster route to zero- and one-dimensional quantum structures by MOCVD", presented at International Workshop of Nitride Semiconductors, Pittsburgh, PA, July 2004.
- J. Han, "MOCVD Growth of III-Nitride Nanostructures", 2004 UKC Conference, Research Triangle, NC, August 2004. J. Han, "Frontiers of III-Nitride UV Optoelectronics and Nanostructures", Rensselaer Polytech Institute, Troy, NY, 2004. **(INVITED)**
- J. Han, "III-Nitride UV Optoelectronics and Nanostructures for Solid State Lighting", 3rd international workshop on Opto Semiconductor Technologies for Solid State Lighting, Gwangju, Korea, December 2004 **(INVITED)**
- A. Nurmikko, "GaN based Nanostructures for light emitter applications", Akasaki Research Symposium, Nagoya University, December 2004 (INVITED)
- A. Nurmikko, "Physics of Light Emission from III-nitride periodic nanostructures", International Workshop on Semiconductor Nitrides, Meijo University, Japan, December 2004 (INVITED)
- A.V. Nurmikko, Y.-K. Song, and J.-H. Song, Jung Han, "Control of Spontaneous and Stimulated Emission in Wide Bandgap Semiconductor Nanoarrays", Symposium on Frontiers of Nanoscience, Salt Lake City, April 2005 (INVITED)
- J. Han, "III-Nitride UV Optoelectronics and Nanostructures", Tokyo Institute of Technology, Tokyo, Japan, December 2004
- J. Han, "MOCVD Growth of III-Nitride Nanostructures", AFOSR Workshop, Anchorage, AK, August 2004.
- A. Nurmikko and J. Han, "Ultraviolet LEDs for Versatile Applications", ISBLLED, Gyongju, Korea, March 2004
- L. Chen et al, "Photonic Crystals in InGaN Light Emitters", CLEO, San Francisco, June 2004
- Y. He, et al, "Optical Properties of Sub-100nm Diameter Nanoposts with Embedded InGaN Quantum Well Heterostructures", presented at International Workshop of Nitride Semiconductors, Pittsburgh, PA, July 2004
- L. Chen et al, "High Efficiency Photonic Crystals in InGaN Light Emitters", presented at International Workshop of Nitride Semiconductors, Pittsburgh, PA, July 2004

Publications

1. He,-Y.; Song,-Y.--K.; Nurmikko,-A.-V.; Su,-J.; Gherasimova,-M.; Cui,-G.; Han,-J., "Optically pumped ultraviolet AlGaInN quantum well laser at 340 nm wavelength", Appl. Phys. Lett. 84, 463 (2004)
2. Yiping He, Lu Chen, Y.-K. Song, and A.V. Nurmikko, S.-R. Jeon, Z. Ren, M. Gherasimova, and J. Han, "Optical Properties of Sub-100nm Diameter Nanoposts with Embedded InGaN Quantum Well Heterostructures", Phys. Stat. Sol.(a) (in press)
3. M. Gherasimova, J. Su,. Cui,-G.; Jeon,-S.--R.; Ren,-Z.; Han,-J.; He,-Y.; Y. K. Song, Nurmikko,-A.-V.D. Ciuparu, and L. Pfefferle, "A nanocluster route to zero- and one-dimensional quantum structures by MOCVD", Phys. Stat. Sol.(a) (in press)
4. Gherasimova,-M.; Cui,-G.; Jeon,-S.--R.; Ren,-Z.; Martos,-D.; Han,-J.; He,-Y.; Nurmikko,-A.-V., "Droplet heteroepitaxy of GaN quantum dots by metal-organic chemical vapor deposition", Appl. Phys. Lett. 85, 2346 (2004)
5. J. Su, G. Cui, M. Gherasimova, H. Tsukamoto, J. Han, D. Ciuparu, S. Lim, L. Pfefferle Y. He, A. V. Nurmikko C. Broadbridge, and A. Lehman, "Catalytic growth of GaN Nanowires and Nanostructures by Metal-Organic Chemical Vapor Deposition", Appl. Phys. Lett., Jan 3 (2005)
6. J. Su, G. Cui, M. Gherasimova, H. Tsukamoto, J. Han, D. Ciuparu, S. Lim, L. Pfefferle Y. He, A. V. Nurmikko C. Broadbridge, and A. Lehman, "Catalytic growth of GaN Nanowires and Nanostructures by Metal-Organic Chemical Vapor Deposition", Appl. Phys. Lett., 86, 013105 (2005)
7. J. Su, M. Gherasimova, G. Cui, H. Tsukamoto, J. Han, T. Onuma, M. Kurimoto, S. F. Chichibu, C. Broadbridge, A. Lehman, Y. He, and A. V. Nurmikko, "Growth of AlGaN nanowires by Metal-Organic Chemical Vapor Deposition", Appl. Phys. Lett. 87, 183108 (2005)
8. Yiping He, Lu Chen, Y.-K. Song, and A.V. Nurmikko, S.-R. Jeon, Z. Ren, M. Gherasimova, and J. Han, "Optical Properties of Sub-100nm Diameter Nanoposts with Embedded InGaN Quantum Well Heterostructures", Phys. Stat. Sol.(c) 2, 2740 (2005)
9. M. Gherasimova, J. Su,. Cui,-G.; Jeon,-S.--R.; Ren,-Z.; Han,-J.; He,-Y.; Y. K. Song, Nurmikko,-A.-V.D. Ciuparu, and L. Pfefferle, "A nanocluster route to zero- and one-dimensional quantum structures by MOCVD", Phys. Stat. Sol.(c) 2, 2361 (2005)
10. J. Han, K. Kim, J. Su, M. Gherasimova, A. V. Nurmikko, S. F. Chichibu, C. Broadbridge, MOCVD Growth and Characterization of AlGaInN Nanowires and Nanostructures, MRS Symp Proc (2005)
11. J. Han, K. Kim, J. Su, M. Gherasimova, A. V. Nurmikko, S. F. Chichibu, C. Broadbridge, MOCVD Growth and Characterization of AlGaInN Nanowires and Nanostructures, MRS Symp Proc v892, p789 (2006)
12. S. F. Chichibu, A. Uedono, T. Onuma, B. A. Haskell, A. Chakraborty, T. Koyama, P. T. Fini, S. Keller, S. P. Denbaars, J. S. Speck, U.K. Mishra, S. Nakamura, S. Yamaguchi, S. Kamiyama, H. Amano, I. Akasaki, J. Han, and T. Sota , Origin of defect-insensitive emission probability in In-containing (Al,In,Ga)N alloy semiconductors, Nature Materials, 5, 810 (2006)
13. K. Kim, T. Henry, G. Cui, J. Han, T. K. Song, and A. V. Nurmikko, Epitaxial Growth of Aligned GaN Nanowires and Nanobridges, to appear in phys. stat solidi (2007)

REFERENCES

[1] J. J. Wierer, D. A. Steigerwald, M. R. Krames, J. J. O'Shea, M. J. Ludowise, G. Christenson, Y. –C. Shen, C. Lowery, P. S. Martin, S. Subramanya, W. Gotz, N. F. Gardner, R. S. Kern, and S. A. Stockman, "High-power AlGaInN flip-chip lght-emitting diodes," Appl. Phys. Lett. **78**, 3379 (2001).

[2] N. Koguchi, K. Ishige, and S. Takahashi, J. Vac. Sci. Technol. B 11, 787 (1993).

[3] K. Kawasaki, D. Yamazaki, A. Kinoshita, H. Hirayama, K. Tsutsui, and Y. Aoyagi, Appl. Phys. Lett. 79, 2243 (2001).

[4] C.-W. Hu, A. Bell, F. A. Ponce, D. J. Smith, and I. S. T. Tsong, Appl. Phys. Lett. 81, 3236 (2002).

[5] N. Koguchi, S. Takahashi, and T. Chikyow, J. Cryst. Growth 111, 688 (1991).

[6] A. G. Bhuiyan, A. Hashimoto, and A. Yamamoto, J. Appl. Phys. **94**, 2779 (2003).

[7] T. L. Tansley and C. P. Foley, J. Appl. Phys. **59**, 3241 (1986).

[8] T. V. Shubina, S. V. Ivanov, V. N. Jmerik, D. D. Solnyshkov, V. A. Vekshin, P. S. Kop'ev, A. Vasson, J. Leymarie, A. Kavokin, H. Amano, K. Shimono, A. Kasic, and B. Monemar, Phys. Rev. Lett. **92**, 117407 (2004).

[9] V. Yu. Davydov, A. A. Klochikhin, R. P. Seisyan, V. V. Emtsev, S. V. Ivanov, F. Bechstedt, J. Furthmuller, H. Harima, A. V. Mudryi, J. Aderhold, O. Semchinova, J. Graul, Phys. Status Solidi B **229**, R1 (2002); J. Wu, W. Walukiewicz, K. M. Yu, J. W. Ager III, E. E. Haller, H. Lu, W. J. Schaff, Y. Saito, and Y. Nanish, Appl. Phys. Lett. **80**, 3967 (2002).

[10] C. Stampfl, C. G. Van de Walle, D. Vogel, P. Kruger, and J. Pollmann, Phys. Rev. B **61**, R7846 (2000)

[11] M. Yoshimoto, H. Yamamoto, W. Huang, H. Harima, J. Saraie, A. Chayahara, and Y. Horino, Appl. Phys. Lett. **83**, 3480 (2003).

[12] A. G. Bhuiyan, K. Sugita, K. Kasashima, A. Hashimoto, A. Yamamoto, V. Y. Davydov, Appl. Phys. Lett. **83**, 4788 (2003).

[13] J. B. MacChesney, P. M. Bridenbaugh, and P. B. O'Connor, Mater. Res. Bull. **5**, 783 (1970).

[14] B. R. Natarajan, A. H. Eltoukhy, J. E. Green, and T. L. Barr, Thin Solid Films **69**, 217 (1980).

[15] X. Xu, P. Specht, R. Armitage, J. C. Ho, E. R. Weber, and C. Kisielowski, Appl. Phys. Lett. **87**, 092102 (2005).

[16] S.-Y. Kwon, H.J. Kim, H. Na, Y.-W. Kim, H.-C. Seo, H.J. Kim, Y. Shin, E. Yoon, and Y.-S. Park, J. Appl. Phys. **99**, 044906 (2006).

[17] C. Nörenberg, R. A. Oliver, M. G. Martin, L. Allers, M. R. Castell, and G. A. D. Briggs, Phys. Status Solidi A **194**, 536 (2002).

[18] T. Tang, S. Han, W. Jin, X. L. Liu, C. Li, D. H. Zhang, C. W. Zhou, B. Chen, J. Han, and M. Meyyapen, J. Mat. Res. **19**, 423 (2004).

[19] H.J. Kim, H. Na, S.-Y. Kwon, H.-C. Seo, H.J. Kim, Y. Shin, K.-H. Lee, Y.-W. Kim, S. Yoon, H.J. Oh, C. Sone, Y. Park, Y.-H. Cho, Y. Sun, and E. Yoon, Phys. Status Solidi C **0**, 2834 (2003)

[20] JCPDS Card No. 06-0416 (ICDD, 1998).

[21] S. Luo, W. Zhou, Z. Zhang, J. Shen, L. Liu, W. Ma, X. Zhao, D. Liu, L. Song, Y. Xiang, J. Zhou, S. Xie, and W. Chu, Appl. Phys. Lett. **89**, 093112 (2006).

[22] O. Ambacher, M. S. Brandt, R. Dimitrov, T. Metzger, M. Stutzmann, R. A. Fischer, A. Miehr, A. Bergmaier, and G. Dollinger, J. Vac. Sci. Technol. B **14**, 3532 (1996).

[23] D. D. Koleske, A. E. Wickenden, R. L. Henry, M. E. Twigg, J. C. Culbertson, and R. J. Gorman, Appl. Phys. Lett. **73**, 2018 (1998).

[24] A. Koukitu, T. Taki, N. Takahasi, and H. Seki, J. Cryst. Growth **197**, 99 (1999).

[25] V. Cimalla, J. Pezoldt, G. Ecke, R. Kosiba, O. Ambacher, L. Speiβ, G. Teichert, H. Lu, and W. J. Schaff, Appl. Phys. Lett. **83**, 3468 (2003).

[26] M. Drago, P. Vogt, and W. Richter, Phys. Status Solidi A **203**, 116 (2006).

[27]For example, C. Chen, C. Yeh, C.Chen, M. Yu, H. Liu, J. Wu, K. Chen, L. Chen, J. Peng,and Y Chen, J. Am. Chem. Soc., 123, 2791 (2001).

[28]G.B. Stringfellow, Mat. Sci. and Eng. B 87, 97 (2001).

[29] H. Choi, J. C. Johnson, R. He, S. Lee, F. Kim, P. Pauzauskie, J. Goldberger, R.J. Saykally, and P. Yang J. Phys. Chem. 107, 8721(2003)

[30] R. S. Wagner in *Whisker Technology*, edited by A. P. Levitt, John Wiley & Sons, New York (1970)

[31] M. Kasu and N. Kobayashi, J. Cryst. Growth 174, 513 (1997)

[32] L. E. Jensen, M. T. Bjork, S. Jeppesen, A.I. Persson, B.J. Ohlsson, and L. Samuelson Nano Lett. 4, 1961(2004)

[33] M. Gherasimova, G. Cui, Z. Ren, J. Su, X. Wang, J. Han, K. Higashimine, and N. Otsuka J. Appl. Phys. 95, 2921(2004)

[34] T. Detchprohm, S. Sano, S. Mochizuki, S. Kamiyama, H. Amano, and I. Akasaki Phys. Stat. Sol. (a) 188 799(2001)

[35] F. Qian, Y. Li, S. Gradecak, D. Wang, C. Barrelet, and C. M. Lieber Nano Lett. 4, 1975(2004)

[36] K. Hiramatsu, K. Nishiyama, A. Motogaito, H. Miyake, Y. Iyecika, and T. Maeda Phys. Stat. Sol. A 176, 535(1999)

[37] D. Du, D. J. Srolovitz, M. E. Coltrin, and C.C. Mitchell, unpublished paper.

[38] Y. Wu, Y. Cui, L. Huynh, C. J. Barrelet, D.C. Bell, and C.M. Lieber Nano Lett. 4, 433(2004)

[39] S. Heikman, S. Keller, S. P. Benbaars, U.K. Mishra, F. Bertram, and J. Christen Jpn. J. Appl. Phys. 42, 6276(2003)

[40] A. P. Alivisatos Science 271, 933(1996)

[41] H. Amano, M. Iwaya, N. Hayashi, T. Kashima, S. Nitta, C. Wetzel, and I. Akasaki, "Control of dislocations and stress in AlGaN on sapphire using a low temperature interlayer", *phys. stat. sol. (b),* vol. 216, pp. 683-689, Nov. 1999.

[42] J. Han, K. E. Waldrip, S. R. Lee, J. J. Figiel, S. J. Hearne, G. A. Petersen, and S. M. Myers, "Control and elimination of cracking of AlGaN using low-temperature AlGaN interlayers," *Appl. Phys. Lett.,* vol. 78, pp. 67–69, Jan. 2001